Title
Faulting processes in active faults – Evidences from TCDP and SAFOD drill core samples

Authors
Janssen, C
Wirth, R
Wenk, H-R
et al.

Publication Date
2014-08-01

DOI
10.1016/j.jsg.2014.04.004

Peer reviewed

Journal of Structural Geology 65 (2014) 100–116

Contents lists available at ScienceDirect

Journal of Structural Geology

journal homepage: www.elsevier.com/locate/jsg

Faulting processes in active faults – Evidences from TCDP and SAFOD drill core samples

C. Janssen [a,*], R. Wirth [a], H.-R. Wenk [b], L. Morales [a], R. Naumann [a], M. Kienast [a], S.-R. Song [c], G. Dresen [a]

[a] GeoForschungsZentrum Potsdam, Telegrafenberg, Potsdam 14473, Germany
[b] Department of Earth and Planetary Science, University of California, Berkeley, CA 94720, USA
[c] Department of Geosciences, National Taiwan University, P.O. Box 13-318, Taipei 106, Taiwan, No. 1, Sec 4, Roosevelt Road, Taipei 106, Taiwan

ARTICLE INFO

Article history:
Received 22 January 2014
Received in revised form
1 April 2014
Accepted 10 April 2014
Available online 5 May 2014

Keywords:
SAFOD
TCDP
Microstructures
Fault rock composition
CPO
EBSD

ABSTRACT

The microstructures, mineralogy and chemistry of representative samples collected from the cores of the San Andreas Fault drill hole (SAFOD) and the Taiwan Chelungpu-Fault Drilling project (TCDP) have been studied using optical microscopy, TEM, SEM, XRD and XRF analyses. SAFOD samples provide a transect across undeformed host rock, the fault damage zone and currently active deforming zones of the San Andreas Fault. TCDP samples are retrieved from the principal slip zone (PSZ) and from the surrounding damage zone of the Chelungpu Fault. Substantial differences exist in the clay mineralogy of SAFOD and TCDP fault gouge samples. Amorphous material has been observed in SAFOD as well as TCDP samples. In line with previous publications, we propose that melt, observed in TCDP black gouge samples, was produced by seismic slip (melt origin) whereas amorphous material in SAFOD samples was formed by comminution of grains (crush origin) rather than by melting. Dauphiné twins in quartz grains of SAFOD and TCDP samples may indicate high seismic stress. The differences in the crystallographic preferred orientation of calcite between SAFOD and TCDP samples are significant. Microstructures resulting from dissolution–precipitation processes were observed in both faults but are more frequently found in SAFOD samples than in TCDP fault rocks. As already described for many other fault zones clay-gouge fabrics are quite weak in SAFOD and TCDP samples. Clay-clast aggregates (CCAs), proposed to indicate frictional heating and thermal pressurization, occur in material taken from the PSZ of the Chelungpu Fault, as well as within and outside of the SAFOD deforming zones, indicating that these microstructures were formed over a wide range of slip rates.

1. Introduction

A key question of fault mechanics is related to the transition between seismic and aseismic slip. For example, many authors assume that the transition from aseismic creep at shallow depth to seismic slip occurs at depth between 5 and 15 km and has been attributed to the dehydration of smectite–illite (e.g. Hyndman et al., 1997; Saffer and Marone, 2003; Marone and Saffer, 2007). The lack of earthquakes at shallow depth can be related to the velocity-strengthening behavior of phyllosilicate-rich gouges (Imber et al., 2008; Ikari et al., 2011). However, the 2011 Tohoku megathrust earthquake has propagated through the shallow part of the subduction zone to the sea-floor surface (Ozawa et al., 2011; Kodaira et al., 2012).

Even though the analysis of fresh fault rocks has received increasing attention, physical mechanisms governing co-seismic slip and aseismic creep remain still elusive due to limited access of microstructures and their relation to co-seismic and aseismic slip. As a consequence of this gap was that several international fault zone drilling projects have started to address fundamental questions about physical and chemical processes controlling faulting and earthquake generation (e.g. Hickman et al., 2004; Song et al., 2007; Zoback et al., 2007, 2010; Boullier, 2011).

This paper is structured around a combined analysis of core samples from two drilling projects (San Andreas Fault Observatory at Depth/SAFOD; Taiwan Chelungpu-fault Drilling project/TCDP). Both allow to identify key similarities and differences between characteristic microstructures of slip zones recently formed by co-seismic processes in earthquake faults (TCDP) or by active creep

* Corresponding author.
E-mail address: jans@gfz-potsdam.de (C. Janssen).

http://dx.doi.org/10.1016/j.jsg.2014.04.004
0191-8141/

(SAFOD). Thus, by examining microstructures in SAFOD and TCDP core samples we may clarify which processes control and trigger creep processes and seismic slip events, respectively. Furthermore we expect that our comparative study of gouge/ultracataclastic material will provide more general insights into key structural features of slip zones controlling the physical and chemical conditions of fault zone deformation. In order to meet this objective, we represent a survey of available data combined with new investigations.

The focus of our study is the comparison of fault rock composition and dominant microstructures (e.g. amorphous material/melt, brittle fracturing, dissolution–precipitation processes, intracrystalline plasticity, clay fabric) in SAFOD and TCDP core samples. To characterize the microstructures we will predominantly use transmission electron microscopy (TEM) and scanning electron microscopy (SEM) combined with focused ion beam techniques (FIB) (Janssen et al., 2010, 2011). Further analytical techniques include X-ray diffraction (XRD) and X-ray fluorescence (XRF) analyses, cathodoluminescence (CL) optical microscopy and electron back-scatter diffraction (EBSD).

2. Methods

XRD and XRF were used to analyze fault rock composition. All samples were dried and ground to a fine powder before analysis. X-ray diffraction analyses were conducted on air dried oriented clay slides before and after treatment with ethylene glycol and heating at 400 °C. X-ray patterns for TCDP and SAFOD samples were collected using a Siemens D5000 powder diffractometer and a diffractometer XRD 3000 TT (Seifert), respectively. The diffraction data for the Siemens diffractometer were recorded from 4° to 75° 2Θ with a step width of 0.02 and a counting time of 4 s per step and for the Seifert diffractometer from 3° to 70° 2Θ with a step width of 0.023/0.4, respectively. For the quantitative analysis of selected samples we determined the relative amounts of phases in a mixture by referencing peak intensity with Ni as an internal standard. Microstructures were investigated with a petrographic microscope, a FEI Quanta 3D scanning electron microscope (SEM) combined with focused ion beam (FIB, dual-beam machine), and a FEI Tecnai G2 F20 X-Twin transmission electron microscope (TEM/AEM) equipped with a Gatan Tridiem energy filter, a Fishione high-angle annular dark field detector (HAADF), and an energy dispersive X-ray analyzer (EDS) to determine chemical composition. The samples for TEM studies were prepared with a focused ion beam (FIB) device (FEI FIB200TEM) at GeoForschungsZentrum (GFZ) (for more details see Wirth, 2004, 2009). The cutting of foils with the FIB allows identification of microstructures down to the nm scale while minimizing preparation induced damage. TEM foils studied here were taken from thin sections that were oriented parallel or normal to the core axis.

To determine the crystallographic orientation of clay minerals, synchrotron X-ray diffraction measurements were conducted at the high-energy beamline BESSRC 11-ID-C of the Advanced Photon Source (APS) of Argonne National Laboratory. A monochromatic X-ray beam with a wavelength of 0.107863 Å and 1×1 mm in size was used. Diffraction images were recorded with a MAR345 image plate detector. Details of sample preparation, diffraction measurements and data analysis are described in Wenk et al. (2008, 2010).

The determination of the calcite crystallographic orientation was carried out by electron back-scatter diffraction (EBSD) in a scanning electron microscope (SEM). For that, we have used standard thin sections polished with diamond paste and colloidal silica. The EBSD measurements were conducted in the FEI Quanta 3D FEG dual-beam machine equipped with EDAX-TSL EBSD camera and OIM software (version 5.31) installed at GFZ-Potsdam. For the EBSD measurements of calcite, we have used an accelerating voltage of 15 kV, beam current of 8 nA, working distance of 15 mm and a stepsize variable between 1 and 0.2 μm. After filtering processes, all measurements with confidence index <0.2 were excluded. Orientation distribution function calculations and plots of pole figures were conducted via the MTEX toolbox for Matlab (Hielscher and Schaeben, 2008; Bachmann et al., 2010).

Note that some samples show considerable heterogeneity and the methods used in this study, such as SEM, TEM, and synchrotron X-ray diffraction investigate small volumes.

3. Structural setting of SAFOD and TCDP samples

The San Andreas Fault (SAF) as well as the Chelungpu-Fault intersect similar types of country rocks, however the fault zone character differs considerably between both faults, notably the very different width of the SAFOD creeping zones and the TCDP principal slip zone, respectively (Table 1). The wider fault gouges of the SAF are likely caused by the cumulative displacement, which is much greater along the SAF than along the Chelungpu fault (Zoback et al., 2010).

3.1. The SAFOD project

The San Andreas Fault Observatory at Depth (SAFOD) is a 3.2 km deep borehole observatory. It was drilled into the San Andreas Fault Zone (SAF, Fig. 1a; Table 1) to study directly the structure and composition of the active San Andreas Fault (Hickman et al., 2007). The drill site is located at the transition between the locked (i.e., seismogenic) segment to the southeast and creeping segment to the northwest (Fig. 1a; Zoback et al., 2011). Within the SAFOD drill holes four major geological units have been identified (Bradbury et al., 2007) with Quaternary and Tertiary sediments, Salinian granite and arkosic sediments beneath the Buzzard Canyon fault. Approximately 1200 m NE of the drill site the arkosic sediments of the Salinian block (Pacific plate) are replaced by shales and siltstones of the Great Valley/Franciscan sequence (North American plate). The lithological boundary may represent an ancestral trace of the SAF (Holdsworth et al., 2011). The main drill hole crosscuts multiple faults including two actively creeping strands, the Southwest Deforming Zone (SDZ) and the Central Deforming Zone (CDZ) (Fig. 1b; Zoback et al., 2010), which were revealed by pronounced and ongoing casing deformation (Bradbury et al., 2007; Zoback et al., 2010). Detailed descriptions of SAFOD Phase 3 core material from Holes E and G (Fig. 1c) are given by Bradbury et al. (2011), Holdsworth et al. (2011), Hadizadeh et al. (2012), and the SAFOD Core Photo Atlas (2010). The temperature at the depths of Hole G core recovery (2.65–2.7 km vertical depth) was 110–115 °C (Lockner et al., 2011; compare also Schleicher et al., 2009).

The findings presented here are based on XRD/XRF, TEM and SEM microstructural studies of 14 representative SAFOD samples that will provide the first continuous high-resolution profile across undeformed host rock and the fault damage zone including gouge from the currently active slip zones (SDZ, CDZ). Apart from sample S1, all investigated SAFOD samples (S2–S14) belong to the Great Valley sequence (Fig. 1c). The samples outside the deforming zones are foliated siltstone/shale (ultra) cataclasites recovered from different depths of the main borehole (3191–3303 m). For a more detailed description of the gouge (deforming zone) samples see Section 4.1.

3.2. The TCDP project

In order to obtain more details of the physical and chemical behavior of the Chelungpu-fault zone, the Taiwan Chelungpu-fault Drilling Project (TCDP; Fig. 2, Table 1) was initiated. Two boreholes

Table 1
Overview about faulting conditions of the SAFOD and TCDP drilling projects.[a]

Location	Fault type	Vertical sample depth	Max. temperature	Long-term slip rate	Total displacement	Host rock	Fault gouge width
SAFOD	Strike-slip	2.600–2.700 m	100–200 °C	25–39 mm a[a]	560 km	Clay-rich sediments	1.6 and 2.6 m
TCDP	Thrust	~1.111 m	44–46 °C *1.100 °C frictional Temp.*	10–15 mm a[a]	300 m	Clay-rich sediments	2 cm

[a] Compiled from Hill and Dibblee (1953), Lee et al. (2001), Titus et al. (2006) and several other authors; compare text.

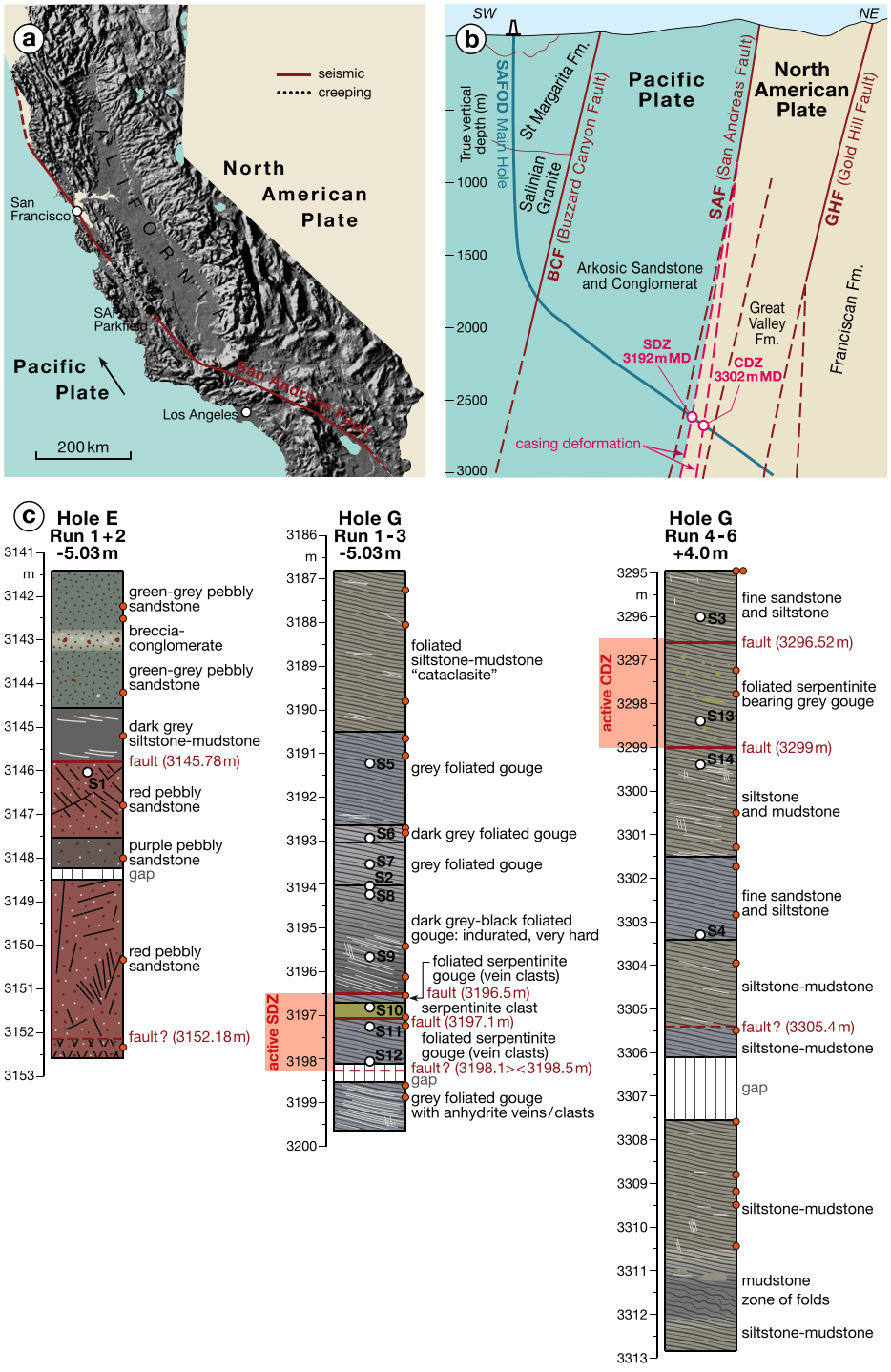

Fig. 1. Location map of the study area. (a) The San Andreas Fault with the SAFOD drill site. The arrow shows the sense of plate movement. (b) Cross section showing the simplified depth profile of the SAFOD main hole (MH) and the SAF and its bifurcation into several strands (slightly modified after Holdsworth et al., 2011) (c) Simplified geological logs of the phase 3 cores (Holdsworth et al., 2011) complemented by the sample positions (S1–S14). Abbreviations: SDZ-Southwest Deforming Zone, CDZ-Central Deforming Zone, MD-measured depth.

(A and B) were drilled in the northern part of the Chelungpu thrust fault where the Chi–chi earthquake (21 September 1999, Mw 7.69) occurred (Yu et al., 2001). The Chelungpu thrust fault is an active fault and part of the fold-and-thrust belt of western Taiwan (Fig. 2a). Both boreholes encountered sandstone, siltstone and shale alternations of late Miocene–Pliocene marine sediments (Fig. 2b) (Song et al., 2007; Boullier et al., 2009). Several fault strands of the Chelungpu-fault system were crossed by TCDP Holes A and B (Fig. 2c) (Ye et al., 2007). The lowermost fault strand at a depth of 1111 m (Hole A) and 1136 m (Hole B) was identified as the principal slip zone (PSZ) associated with 1999 Chi–Chi earthquake (Ma et al., 2006; Kuo et al., 2013). The temperature in the TCDP borehole is about 46 °C at a depth of 1110 m (Mori et al., 2008).

Our TCDP samples were taken from the black gouge zone (BGZ) within the principal slip zone at 1111 m (Hole A, sample TA1) and from the surrounding foliated gouge of Hole A (samples TA2-TA8) and Hole B (samples TB1-TB10) (Fig. 2d). The sampling sections were described in detail by Boullier et al. (2009).

4. Results

4.1. Fault rock composition

The composition of SAFOD and TCDP samples is described extensively in several publications (SAFOD: e.g. Moore and Rymer, 2012; Holdsworth et al., 2011; Bradbury et al., 2011; Mittempergher et al., 2011; TCDP: Ye et al., 2007; Sone et al., 2007; Ishikawa et al., 2008; Boullier et al., 2009). Here we describe selected SAFOD and TCDP samples to illustrate similarities and differences in fault rock

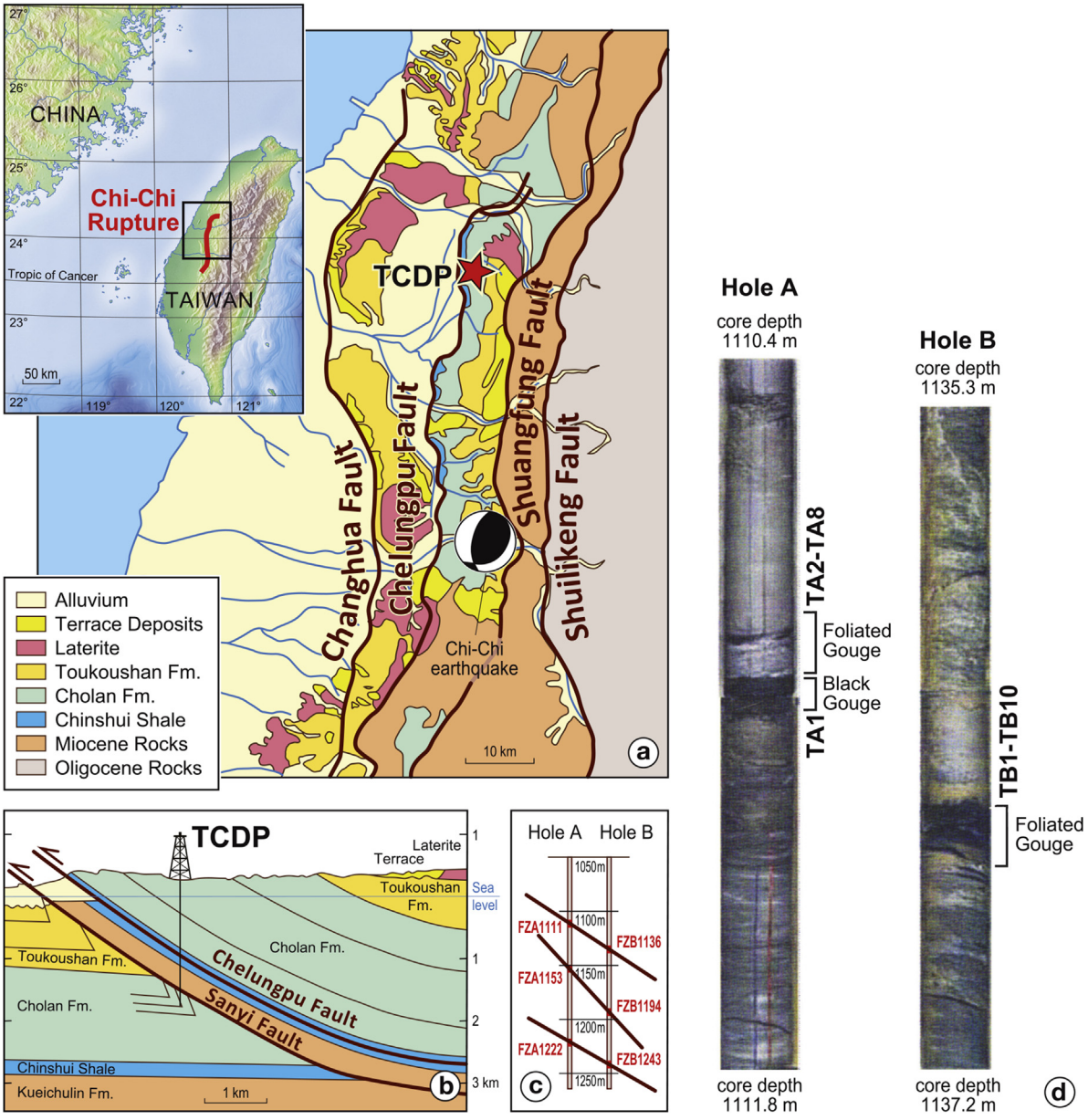

Fig. 2. Geological map and cross section of western Taiwan showing the distribution of major faults (Kuo et al., 2011). The insert shows the geotectonic setting of Taiwan. (a) Geological map with major thrusts. (b) Cross section through the drill site indicating the relation between sediment formation and faults (after Hung et al., 2007). (c) Correlation between the three fault zones observed in Holes A and B (after Hirono et al., 2007). (d) Core images of Holes A and B with sampling locations (TA1, TA2–TA8; TB1–TB10). The drill cores are predominantly composed of siltstones with subsidiary layers of fine-grained sandstone (Song et al., 2007).

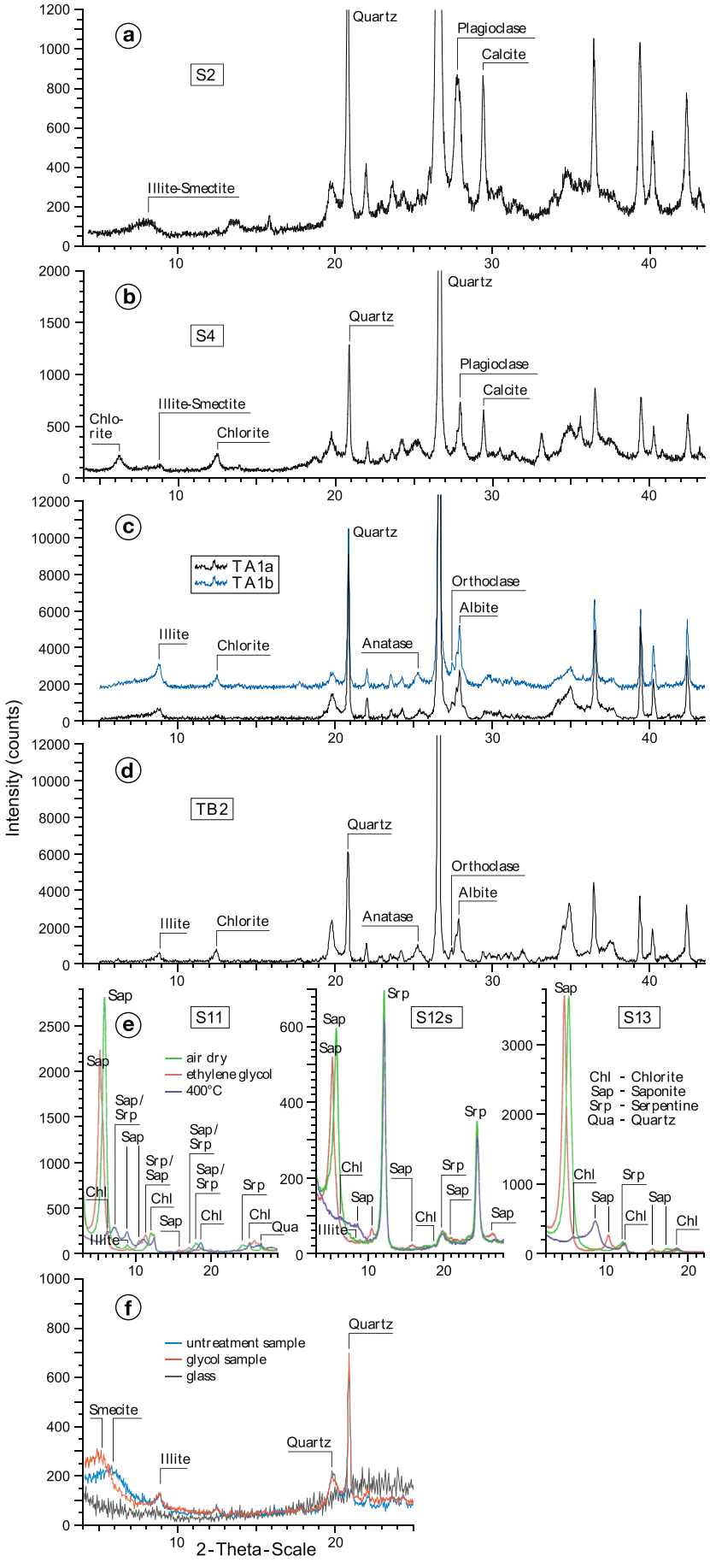
a
S2
Quartz
Plagioclase
Calcite
Illite-Smectite
b
S4
Quartz
Quartz
Plagioclase
Calcite
Chlo-
rite
Illite-Smectite
Chlorite
c
TA1a
TA1b
Quartz
Orthoclase
Albite
Illite
Chlorite
Anatase
d
TB2
Quartz
Orthoclase
Albite
Illite
Chlorite
Anatase
Intensity (counts)
e
S11
S12s
S13
air dry
ethylene glycol
400°C
Sap
Srp
Chl
Qua
Illite
Chl - Chlorite
Sap - Saponite
Srp - Serpentine
Qua - Quartz
f
untreatment sample
glycol sample
glass
Smecite
Illite
Quartz
Quartz
2-Theta-Scale

composition. The major element data of the TCDP samples were taken from Ishikawa et al. (2008).

Representative XRD patterns for the selected SAFOD and TCDP core samples are shown in Fig. 3. The major mineral assemblages of fault rock samples outside of the deforming zones (SAFOD) and principal slip zone (TCDP) respectively, are very similar. Quartz, feldspar and phyllosilicate minerals such as illite, smectites and chlorite are identified as the major mineral constituents (Fig. 3a–d). More detailed studies show substantial differences in the clay-gouge composition of SAFOD and TCDP samples, respectively (Fig. 3e–f). For instance, clay minerals from the SAFOD–SDZ (samples S11, S12s) and SAFOD–CDZ (sample S13) are identified as serpentine–saponite mixed layers; saponite, chlorite and illite (Fig. 3e, Table 2; see also Holdsworth et al., 2011; Lockner et al., 2011; Moore and Rymer, 2012; Schleicher et al., 2012). Besides clay minerals, serpentine (chrysotile) is a further main constituent of some samples (samples S10, S13; Fig. 3e, Table 2). The TCDP black gouge (samples TA1a-b) and foliated gouge (sample TB2) samples mainly consist of illite and chlorite (Fig. 3c and d), and, in addition, smectite and kaolinite (Kuo et al., 2009). Kuo et al. (2009) describe a drastic decrease of illite toward the principal slip zone, whereas smectites are rare or absent in all portions of the fault zone but become abundant in the principal slip zone (up to 80%; Fig. 3f).

Similar to the XRD results of gouge material, the major and trace-element concentrations differ considerably between SAFOD and TCDP gouge samples measured by XRF. Toward the active deforming zones (SDZ, CDZ) of the SAF, the samples are increasingly enriched in Mg and depleted in Si compared to samples that are located further away (Fig. 4a). The highest Mg-concentration was measured in the SDZ and CDZ (Fig. 4a; compare Bradbury et al., 2011). Neglecting the smaller sample spacing, the TCDP samples do not reveal any dependency of major element concentration on the distance to the BGZ (corresponds to PSZ, Fig. 4b; data from Table 1 in Ishikawa et al., 2008). In contrast, some trace-element concentrations (e.g. Sr, Ba, Li, Rb, Cs), which are very sensitive to fluid–rock interactions, show systematic variations across the BGZ (Fig. 1 in Ishikawa et al., 2008). Their depth profiles of trace-element concentrations exhibit increases of Sr and Ba and decreases of Li, Rb and Cs in the black gouge zone (PSZ) compared to the surrounding rocks, whereas selected trace elements (Sr, Ba, and Rb) in SAFOD samples exhibit no systematic variation across the deforming zones (XRF data in supplementary materials).

4.2. Microstructures

We compared the microstructural record of samples subjected to aseismic and co-seismic slip, giving special emphasis to TEM and SEM investigations.

4.2.1. Amorphous material/melting

Amorphous material, forming pseudotachylites (PT), is assumed to form by frictional melting (melt origin; e.g. Sibson, 1975) or by comminution of grains (crush origin; e.g. Wenk, 1978). Typical textures indicating frictional melting are glassy material, devitrification textures, vesicles and amygdales (e.g. Lin, 1994; Wenk et al., 2000; Ujiie et al., 2007). TEM imaging of SAFOD samples shows amorphous material in ultracataclastic core samples (S2, S3; Fig. 5a) and in gouge material of the deforming zone (S11). But melt textures have not been observed. The composition of the amorphous material is either similar to that of the adjacent matrix or shows a slight enrichment in silica (Fig. 5b; Janssen et al., 2010).

For the Chelungpu fault, pseudotachylites with a glass texture have been found in a shallow drill hole that penetrates the southern part of the fault (Otsuki et al., 2005). Pseudotachylites with typical melt structures (e.g. vesicles, spherulites) have also been described in samples from Hole B of TCDP (Hirono et al., 2006; Otsuki et al., 2009). For Hole A, Kuo et al. (2009, 2011) described pseudotachylites with vesicles of about 1–40 μm diameter within the PSZ (1111-m Zone). Our SEM images of TCDP sample from the black gouge in Hole A (TA1) also revealed amorphous material with vesicles (Fig. 5c).

4.2.2. Dissolution–precipitation processes

Dissolution–precipitation processes are indicated by pressure-solution seams, alteration of minerals and the growth of new minerals (phyllosilicates, calcite cement). Based on our microstructural analysis, pressure-solution features, which are defined by pervasive dark seams of insoluble material (pressure-solution relics) that impart a striping through the rocks, were observed in virtually all thin sections of both SAFOD and TCDP core materials (Fig. 6a and b). TEM observations of SAFOD and TCDP samples reveal partly dissolved quartz and feldspar grains in both sample groups; although grain shapes are different in different samples. Quartz and feldspar grain boundaries in SAFOD samples appear more serrated (Fig. 6c) whereas TCDP samples show more smoother grain boundaries (Fig. 6d).

Fluid-driven alteration reactions in SAFOD and TCDP samples affect quartz and feldspar grains, displaying internal alteration patches, which serve as nucleation sites for phyllosilicates (Fig. 6e and f, white arrows; see also Holdsworth et al., 2011; Hadizadeh et al., 2012; Janssen et al., 2012). These phyllosilicates either show clay particles that are randomly oriented or they are aligned forming face-to-face particle contacts (black arrow in Fig. 6e). Locally, clay flakes are bent, folded or show sigmoidal shapes (black arrow in Fig. 6f), indicating that these clay flakes are deformed (see also section *clay-gouge fabric*). Inter-clay layer pores occur between flakes of phyllosilicates (Fig. 6f; Janssen et al., 2011).

Calcite cement is found in SAFOD as well as in TCDP core samples (Fig. 7a and b). Variations in the cathodoluminescence (CL)-colors are typical for vein and matrix cement (Fig. 7c and d). In SAFOD samples orange–dark orange luminescent calcite predominantly fill veins both within and outside the deforming zones whereas in TCDP samples the matrix of the foliated gouge sample luminescences orange–red.

4.2.3. Deformation of calcite and quartz grains

We found evidence for crystal deformation in both calcite and quartz grains of SAFOD and TCDP samples. The deformation mechanisms include dislocation glide and mechanical twinning in calcite and quartz (Dauphiné twins). For SAFOD samples, internal deformation of calcite crystals within the veins varies from heavily deformed grains to almost undeformed or only slightly deformed grains (Fig. 8a–d). The latter were found outside the deforming zones only. Calcite in the most deformed veins is most strongly twinned (Fig. 8a). The twinned crystals display one, two or three sets of straight or weakly bent twins (Rybacki et al., 2011). A TEM examination of strongly deformed vein cement reveals a high density of straight dislocations, indicating dislocation glide

Fig. 3. Typical X-ray diffraction (XRD) patterns for selected SAFOD and TCDP core samples. (a–b) SAFOD: The (ultra)-cataclastic rocks outside of the deforming zones are composed of quartz, plagioclase, phyllosilicates and calcite. Phyllosilicate minerals include illite–smectite and chlorite. (c–d) The major constituents of TCDP samples are quartz, albite, orthoclase, anatase, illite, and chlorite. (e) Samples from the SAFOD deforming zones (SDZ and CDZ) contain besides chlorite and saponite, serpentine. (f) Sample of the PSZ (TCDP; Figure adapted from Kuo et al., 2009, Fig. 3b).

Table 2
Composition of selected SAFOD samples.

Composition	S10, SDZ [in vol %]	S11, SDZ [in vol %]	S12s, SDZ [in vol %]	S13, CDZ [in vol %]
Quartz	–	14	0.2	4
K-Feldspar		1	–	1
Plagioclase	–	4	0	2
Calcite	7.5	1	0.3	2
Serpentine/saponite ml	–	72	10.5	72
Serpentine (chrysotile)	84.5	–	88	15.5
Chlorite	–	4	0.5	3
Illite	–	4	0.5	–
Pyrite	–	–	–	0.5
Amorphous material	8	–	–	–

(Fig. 8c). In comparison, the weakly deformed calcite grains show no twins and only few dislocations (Fig. 8b and d).

For the TCDP matrix cement, observations by optical microscopy and TEM reveal significant differences in the intensity of crystal plastic deformation of calcite. Under cross-polarized light, the calcite matrix of the foliated gouge sample is only weakly twinned (Fig. 8e). However, at the TEM scale the same calcite crystals are characterized by a high dislocation density and Moiré patterns (Fig. 8f). Dauphiné twins in quartz have been detected in TEM images of both SAFOD and TCDP samples (Fig. 8g and h). In SAFOD samples, few quartz grains outside the deforming zones contain Dauphiné twins, whereas in TCDP samples only quartz grains from the black gouge are twinned.

4.2.4. Calcite and quartz fabric

EBSD analysis of crystallographic preferred orientation (CPO) of calcite and quartz was performed only on one SAFOD (S6; calcite only) as well as one TCDP sample (TA2). The CPO of calcite differs markedly between SAFOD and TCDP samples (Fig. 9). The results for the SAFOD sample indicate some vein-calcite grains with a moderate to weak preferred orientation of the [0001] axes while the poles of other crystallographic planes more randomly distributed (Fig. 9a and b). The distribution of misorientation angles shows the intense presence of subgrains (misorientations between 3 and 10°) and e-twinning (misorientations between 70 and 80° parallel to [0–221] axis; Fig. 9c). It is important to note that part of the SAFOD CPO of calcite veins is related to development of twins. In contrast, both calcite and quartz from the matrix of the studied TCDP sample are randomly oriented (Fig. 9d–g).

4.2.5. Clay-gouge fabric

Clay microfabrics were analyzed using optical microscopy, scanning electron microscopy (SEM), transmission electron microscopy (TEM), and synchrotron X-ray diffraction measurements. The latter was performed only on one gouge sample of each sample group (SAFOD: S2; TCDP: TA2). In general, samples are very heterogenous and coarse-grained with abundant quartz and fragments of plagioclase, which contribute discrete spots to diffraction patterns rendering a quantitative analysis impossible. The optical inspection displays a sub-parallel alignment of clay particles for both sample groups (Fig. 10a and b). However, a qualitative inspection of synchrotron diffraction patterns averaged over 1 mm indicates that only a weak preferred orientation of phyllosilicates is present in SAFOD as well as TCDP gouge samples (Fig. 10c and d). The dominant dark rings in the diffraction patterns correspond to quartz (Q100 and Q101 are labeled in Fig. 10e). The diffuse rings at a d-spacing = 10 Å correspond to illite/smectite overlapped with the illite/mica peak. The Rietveld (1969) analysis (Wenk et al., 2010) of diffraction images established that of phyllosilicates are basically random with maxima less than 1.05 multiples of random

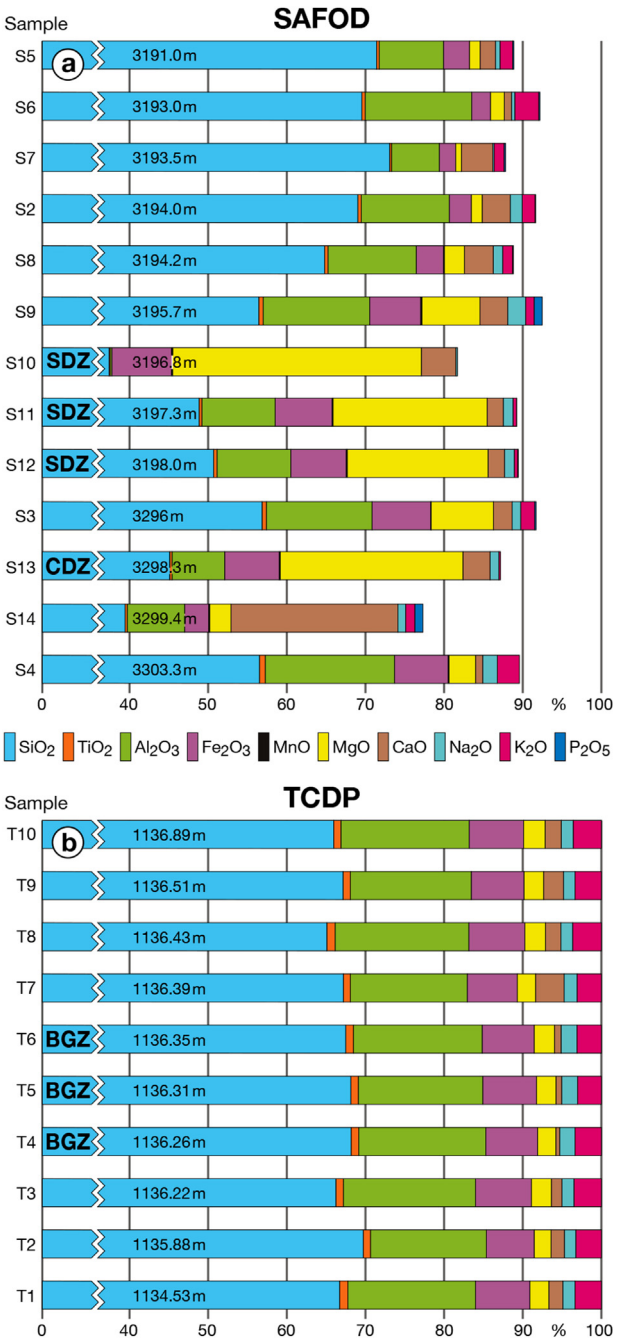

Fig. 4. Results of X-ray fluorescence analyses of (a) SAFOD and (b) TCDP samples illustrating the major and minor elements of the fault rocks (SAFOD data without H_2O and CO_2; TCDP figure is based on sample data from Table 1 in Ishikawa et al., 2008; these samples were collected from TCDP Hole B; samples T4–T6 belong to the black gouge zone/BGZ). The listed depths of SAFO samples match the SAFOD Core Photo Atlas (2010).

distribution. For comparison we show a similar image for Kimmeridge shale in Fig. 10e where preferred orientation of illite–mica (IM200) is 6.5 m.r.d. and of kaolinite (K001) 5 m.r.d. (Vasin et al., 2013). SEM and TEM observations show a clear distinction between a strong clay fabric in local (μm) slip zones ("slip-zone fabric"; Fig. 11a and b) and randomly oriented (newly formed) clay particles (Fig. 11c and d), dominating the fault matrix ("matrix fabric"; Janssen et al., 2012), in all samples of both groups. Fault-related deformation on the particle scale is characterized by kinking and rotation of sheet silicates (Fig. 11e and f).

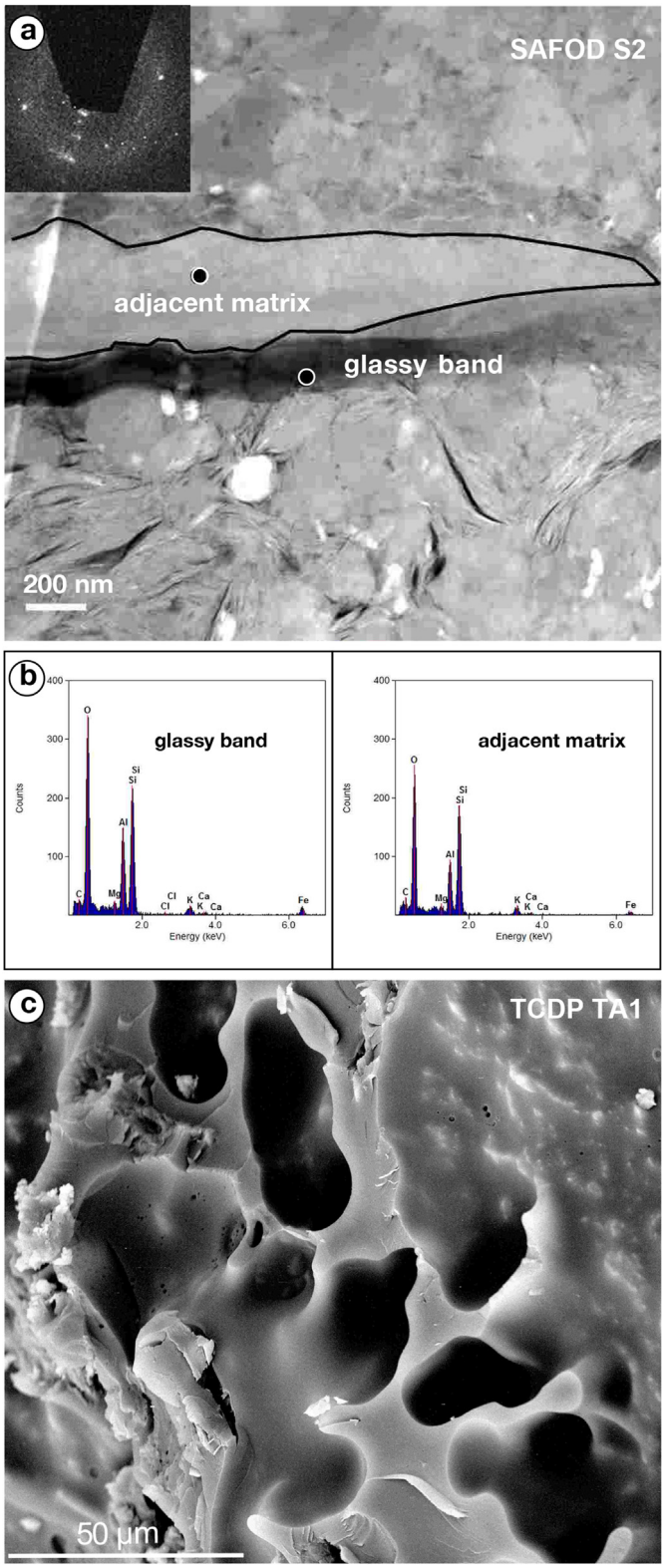

Fig. 5. TEM and SEM micrographs illustrating the presence of amorphous material and melt structures respectively in SAFOD and TCDP samples. (a) TEM high-angle annular dark field (HAADF) image illustrates an amorphous layer in the ultracataclastic matrix. The upper-left corner shows diffuse broad scattering intensity from non-crystalline material in addition to some individual reflections from crystals. (b) EDX spectra acquired from glassy band and host rock material (Fig. 5a and b is adopted from Janssen et al., 2010, Fig. 3). (c) SEM micrograph shows vesicles in a TCDP sample from the principal slip zone indicating frictional melting.

4.2.6. Clay-clast aggregates

Spherical clasts coated by a clay cortex are termed clay-clast aggregates (CCAs; Boutareaud et al., 2008). CCAs in SAFOD and TCDP samples were detected at the micro and nanometer scale (Fig. 12). Contrary to the TCDP samples, where CCAs only occur in the black gouge (sample TA1), our microstructural analysis of SAFOD samples identified several CCAs within and outside of the deforming zones. In more detail, TEM images from several SAFOD and TCDP samples illustrate that numerous rounded or angular clasts are wrapped by sheet silicates (Fig. 12a and b). The central clast is mostly composed of quartz or feldspar whereas the thin clay cortex is composed of illite–smectite mixed layers.

5. Discussion

5.1. Fault rock composition

The host rock composition of the San Andreas Fault zone is comparable with the Chelungpu fault. Both faults cut through a sedimentary sequence built up from alternating silts and shales. Differences in the clay-gouge composition of SAFOD and TCDP samples as revealed in XRD and XRF data may be attributed to different sample depths, and temperatures and, possibly, contrasting faulting regimes (Table 1). Moore and Rymer (2012) suggest that the Mg-bearing clays in the gouges of SAFOD samples from the deforming zones are formed by metasomatic reactions between serpentine entrained in the fault and adjoining sedimentary rocks. Many previous studies suggest that the growth of Mg-rich phyllosilicates may play a key role in the mechanical behavior of the SAF and can be directly related to fault weakening (e.g. Moore and Rymer, 2007, 2012; Schleicher et al., 2010; Holdsworth et al., 2011; Bradbury et al., 2011; Lockner et al., 2011). Janssen et al. (2011) suggest that the presence of abundant clay minerals is often related to the occurrence of nanoscale porosity that may indicates high fluid pressure.

The presence of chlorite–smectite in samples of the SAFOD deforming zones extends the potential role of mineralogical processes in fault weakening to depth up to 10 km (Schleicher et al., 2012). In addition, also the results of laboratory strength measurements of SAFOD core material provide strong evidence that the deformation of the creeping portion of the SAF is controlled by the presence of weak clay minerals (here saponite; Lockner et al., 2011; Van der Pluijm, 2012). Other friction experiments show that fault weakness can occur in cases where weak mineral phases (phyllosilicates) constitute only a small percentage of the total fault rock assemblage (Collettini et al., 2009).

To explain the smectite abundance in the PSZ of the Chelungpu fault, Kuo et al. (2009) assumed that frictional heat may have caused mineral melting and later pseudotachylite was altered to smectite. The systematic variations in trace-element concentrations across the PSZ of the Chelungpu fault suggest that high temperature fluids (above 350 °C) derived from heating of sediment pore fluids during the earthquake interact with fault rocks and mobilized trace elements (Ishikawa et al., 2008). The authors assumed that this effect may stimulate thermal pressurization and cause fault weakening. In contrast, trace-element concentrations in SAFOD samples provide no indications that fault gouges in the deforming zones were subjected to temperatures above 350 °C.

The presence of clay-gouge layers in fault cores of both the SAF and Chelungpu fault (irrespective of their different composition) is consistent with many fault zone studies that identified clay minerals as an important agent possibly controlling fault mechanics and fluid flow (e.g. Warr and Cox, 2001; Boullier et al., 2009, 2011; Schleicher et al., 2009; Moore and Rymer, 2012).

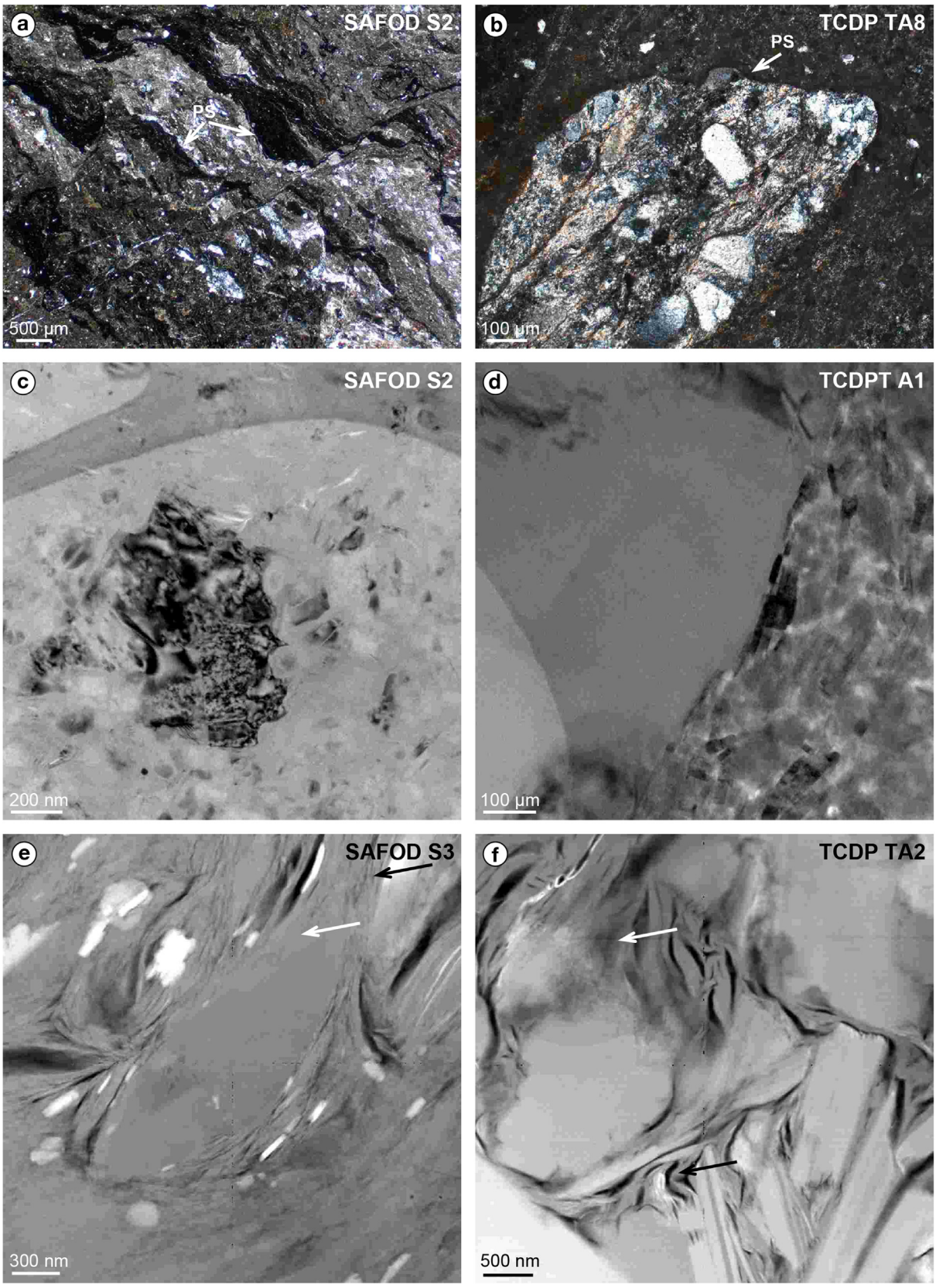

Fig. 6. Illustrative examples of dissolution–precipitation patterns. (a) and (b) Microscopic images of a clay-rich matrix with dark pressure-solution seams in SAFOD and TCDP samples. PS = Pressure-solution seam. (c) and (d) TEM micrographs of quartz grains with dissolved (SAFOD) and smooth (TCDP) grain boundaries. (e) and (f) TEM micrographs of dissolved quartz grains with newly formed clay minerals in SAFOD and TCDP samples. The arrows indicate the transition from the dissolved grain boundary to the newly formed grains.

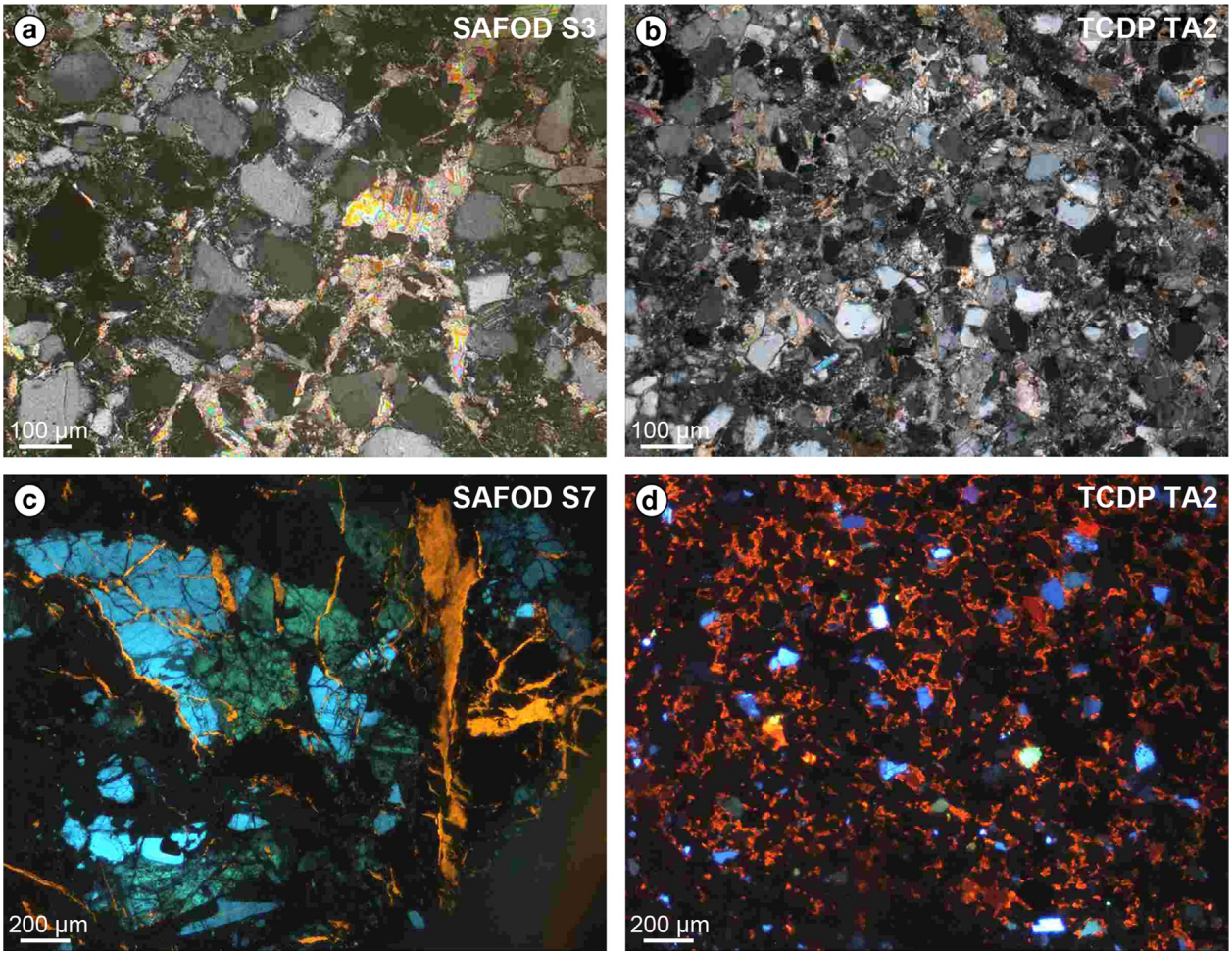

Fig. 7. Low magnification photomicrographs of calcite cement. (a) and (b) Calcite cement of SAFOD and TCDP samples under crossed polarizers. In both samples, the calcite cement is weakly to moderately deformed. (c) and (d) Cathodoluminescence (CL) photomicrographs showing precipitation of vein- (SAFOD) and matrix- (TCDP) calcite cement.

5.2. Microstructures

Evaluation of the microstructural record in ultracataclastic rocks (damage zone samples) and gouge material of SAFOD and TCDP core samples reveals a complex picture and deformation characteristics often can not be assigned unambiguously to either seismic or aseismic faulting processes.

5.2.1. Amorphous material/melting

Field and laboratory studies have shown that pseudotachylites produced by frictional melting contribute to co-seismic weakening (Sibson, 1975; Goldsby and Tullis, 2002; Di Toro et al., 2004). The occurrence of glass textures in TCDP samples from Holes A and B clearly shows that frictional melting occurred. Kuo et al. (2011) estimated a temperature range from 900 °C to 1100 °C of co-seismic heating in clay-rich fault gouges of the Chelungpu-fault zone. Kuo et al. (2009) suggested that pseudotachylites developed during the 1999 Chi–Chi earthquake, were quickly altered to smectite.

Contrary to the Chelungpu fault, the origin of amorphous material in SAFOD samples is not clear. Janssen et al. (2010) assumed that the amorphous material may be related to a crushing and comminution process rather than to rapid cooling of melt. The authors speculated that the observed amorphous phases may act as lubricating layers that reduce friction in the San Andreas Fault. Kirkpatrick et al. (2013) reported that natural silica gel, coating fault surfaces of the Corona Heights fault, could act as a dynamic weakening mechanism in faults at shallow crustal conditions. In general frictional melts/pseudotachylites are rare in fault rocks (Toy et al., 2011). It is conceivable that alteration processes during post-seismic deformation may have obliterated structures produced during seismic slip (Di Toro et al., 2006).

5.2.2. Dissolution–precipitation processes

Dissolution–precipitation is commonly observed in clay-rich fault gouges and is considered an important deformation mechanism accumulating fault slip (Gratier et al., 2011). Dissolution–precipitation processes are operative during co-seismic and aseismic slip (Gratier and Gamond, 1990; Gratier et al., 2011; Chen et al., 2013). Pressure-solution seams and soluble minerals such as feldspar, quartz and calcite are present in SAFOD as well as TCDP samples. In the SAF, these processes are widespread and favor aseismic pressure-solution creep by the presence of fluids, a high amount of phyllosilicates and by fracturing (Gratier et al., 2011; Moore and Lockner, 2011). Richard et al. (2013) described foliated domains with preferred orientation, formed by pressure-solution creep mechanisms in the damaged zone and foliation without preferential orientation in the CDZ. Janssen et al. (2011) supposed that porosity was enhanced by dissolution and precipitation reactions and the formation of alteration products (clay minerals).

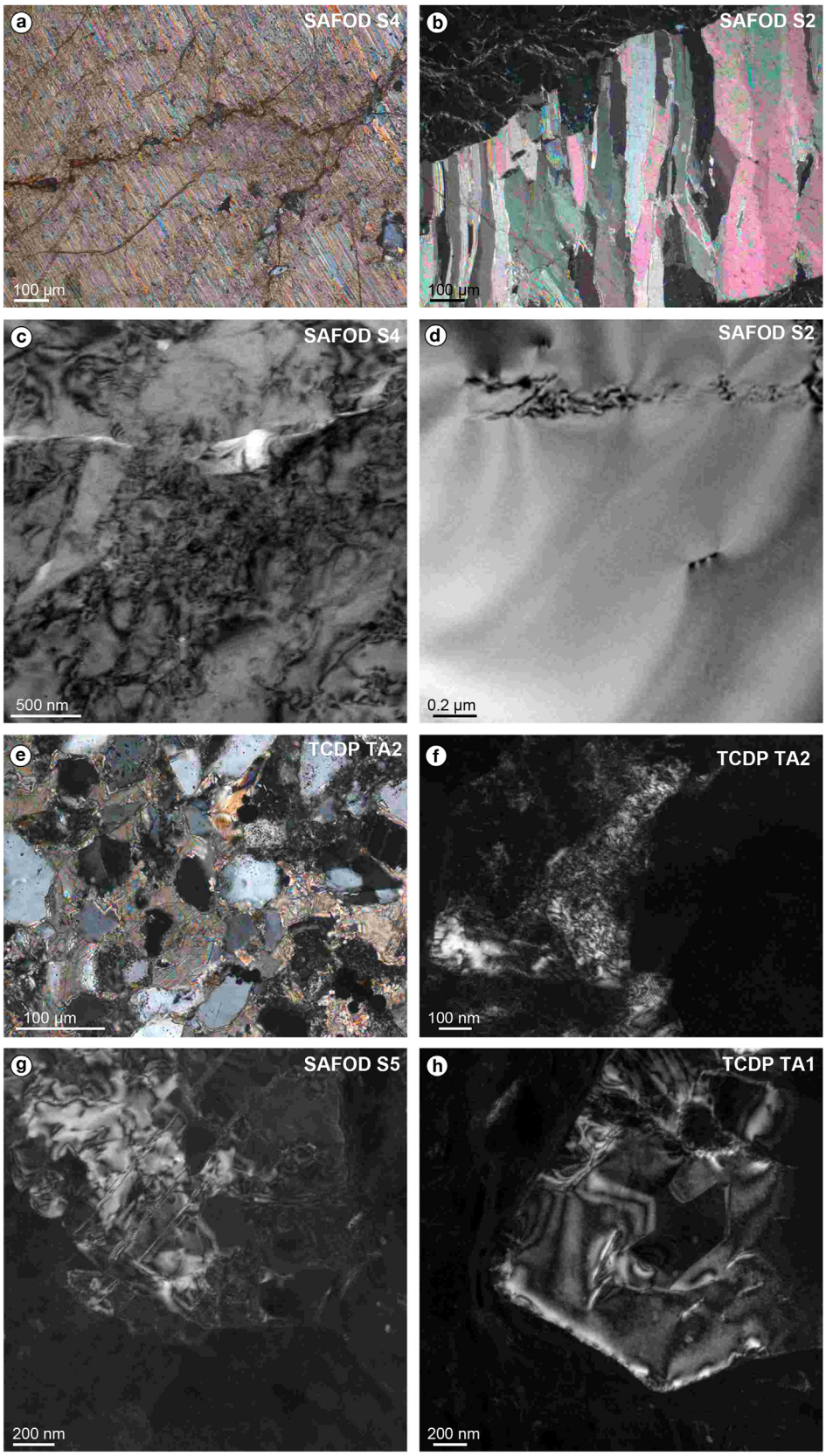

Fig. 8. Microphotographs showing characteristic deformation mechanisms in calcite and quartz grains. (a) Twinned vein cement with straight twins, dissected by stylolitic seams. (b) Fibrous calcite crystals are not twinned and not fractured, indicating that healing processes outlasted the period of brittle faulting. (c) TEM photomicrographs of calcite in SAFOD veins showing examples of strongly deformed grains with high dislocation density and (d) weakly deformed grains with only few dislocations. (e) Microphotograph of weakly twinned calcite cement in a TCDP sample. (f) TEM photomicrograph of the same sample as in (e) reveals a high dislocation density and Moiré patterns. (g) and (h) TEM micrographs illustrating Dauphiné twins in quartz of SAFOD and TCDP fault rocks.

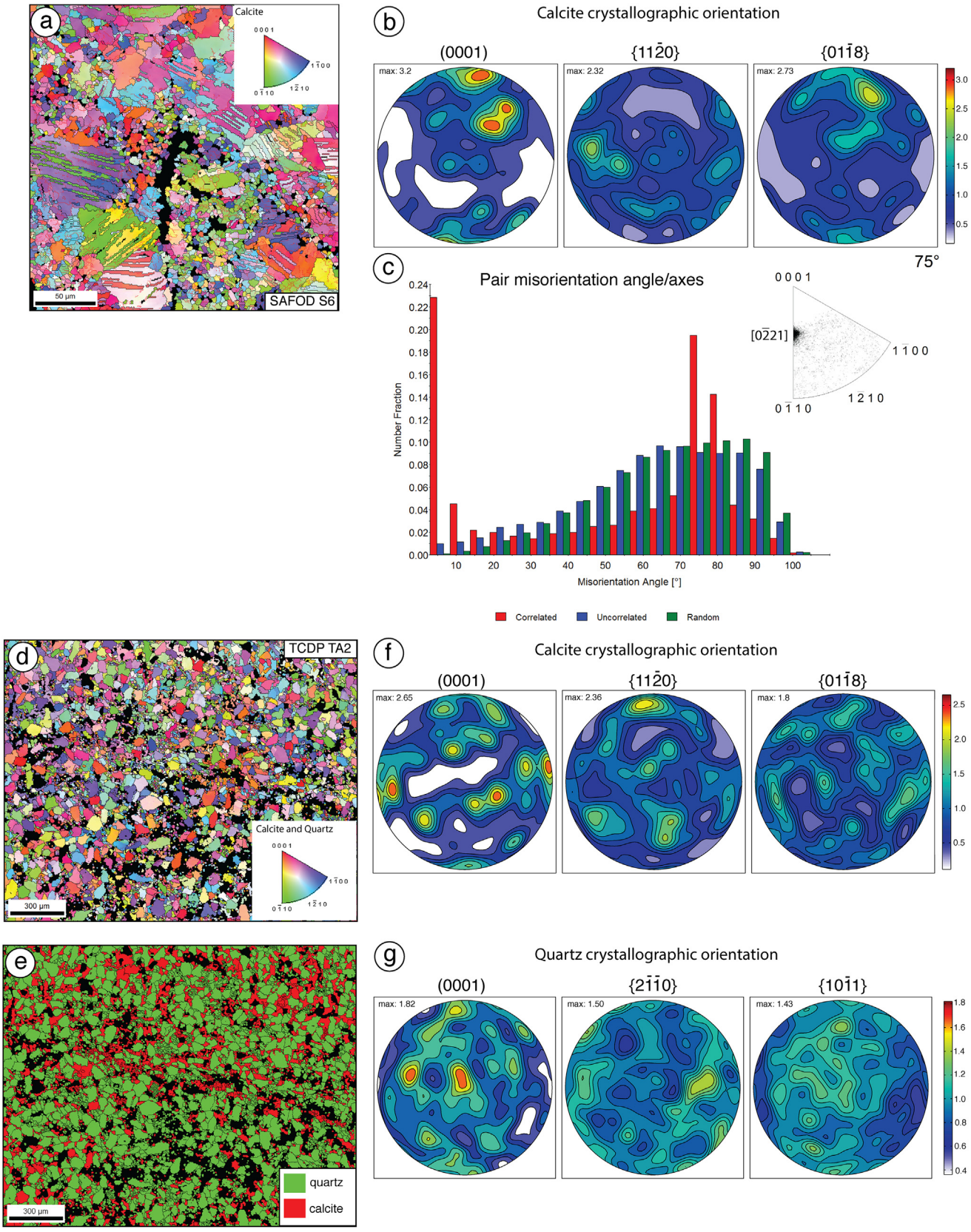

Fig. 9. Crystal orientation maps (EBSD). (a) and (b) Crystallographic preferred orientation of SAFOD vein and matrix calcite. (c) The distribution of misorientation angles for calcite grains (d)–(g) Crystallographic preferred orientation of TCDP matrix calcite and quartz.

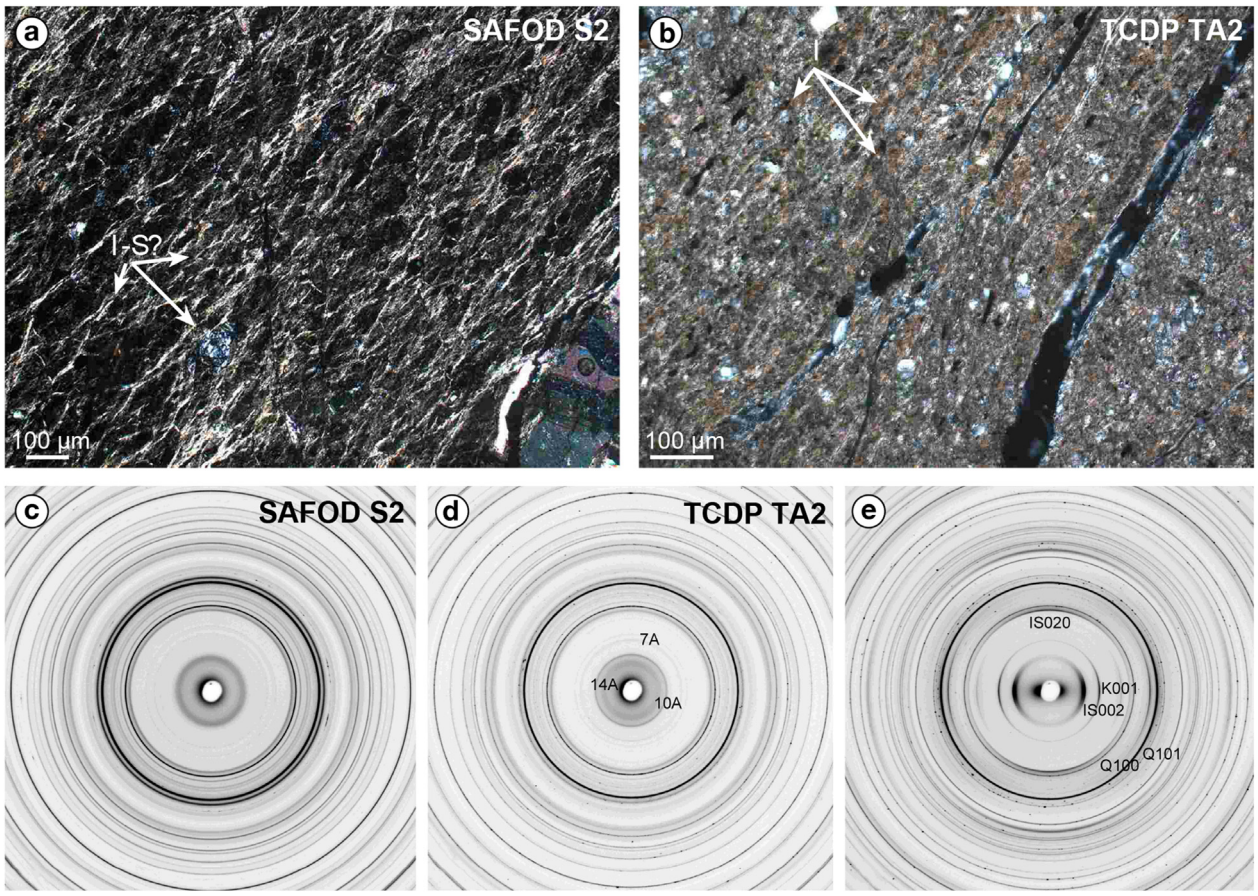

Fig. 10. Illustrative examples of clay-gouge fabrics. (a) and (b) Photomicrographs of sub-parallel aligned clay minerals forming a weak foliation in SAFOD and TCDP samples under crossed polarizer. I–S = illite–smectite; I = illite. (c) and (d) X-ray diffraction images of the same SAFOD and TCDP samples as in (a) and (b). In fault gouge variations are minimal suggesting a random fabric. Lattice spacings indicated in (d) are typical of montmorillonite and chlorite (14), illite–mica (10) and kaolinite (7). (e) X-ray diffraction image of a typical Kimmeridge shale for comparison. In shale azimuthal intensity variations for phyllosilicates (IS illite–smectite, K kaolinite) are indicative of preferred orientation. Quartz (Q) has in all three samples a random fabric.

For TCDP samples, evidence for dissolution–precipitation processes (e.g. dissolved grain boundaries, feldspar alteration, calcite cementation) is less frequently found than in SAFOD fault rocks. This is possibly related to a shallow sampling depth and lower temperatures during inter-seismic periods. In general, we suggest that dissolution–precipitation processes in both fault zones occurred during post- and inter-seismic phases of the earthquake cycle. Newly formed phyllosilicates in SAFOD and TCDP samples, mainly smectites (especially Mg-rich smectite/saponite in SAFOD samples; see above), indicate neocrystallization from hydrothermal fluids. Calcite precipitation in fractures (vein-calcite cement, mainly found in SAFOD samples) and in the matrix (matrix-calcite cement, mainly found in TCDP foliated gouge samples) assist in healing of the fault rocks. Differences in the CL-colors of matrix (TCDP) and vein-calcite cement (SAFOD) indicate multiple episodes of cementation and may reflect different fluid sources.

5.2.3. Deformation in calcite and quartz grains

The variation of internal crystal deformation in the SAFOD calcite veins suggests multiple crack and seal episodes. For instance, the undeformed or slightly deformed calcite vein generation in SAFOD samples outside the creeping zones suggests that late cementation processes outlasted faulting. However, the exact timing of twinning remains unclear. The vein filling with elongated to fibrous calcite has previously been interpreted to indicate a slow opening during creep (Gratier and Gamond, 1990). Dislocation densities and twin line densities in SAFOD samples have been used as paleo-piezometers. The corresponding differential stresses vary between 33 and 132 MPa, deduced from dislocation density and 92–251 MPa obtained from twin density, possibly reflecting chronologically different maximum stress states (Rybacki et al., 2011). Dauphiné twins in SAFOD quartz may indicate episodes of high local stresses on the grain scale that could be attributed to former seismic events, superimposed on the current creep mode of the San Andreas fault at Parkfield (Wenk et al., 2011).

Deformation patterns in TCDP calcites are difficult to interpret. In thin sections, the only weakly deformed matrix-calcite cement suggests that during seismic faulting deformation was strongly localized in clay-rich parts of the fault rocks. However, TEM images of the same matrix calcites, display high dislocation densities and Moiré patterns. As in the SAFOD sample, Dauphiné twins in TCDP quartz suggest high local stresses, possibly reflecting the 1999 Chi–Chi earthquake.

5.2.4. Calcite fabric

The differences in the calcite fabric patterns of the SAFOD and TCDP samples are significant. The CPO in the SAFOD sample suggests that pervasive aseismic (creeping) deformation promotes the development of a weak to moderate calcite fabric, whereas localized co-seismic deformation at shallow depth does not result in a CPO of the matrix calcite in TCDP samples. Our findings agree with previous investigations, which suggested that the CPO developed at

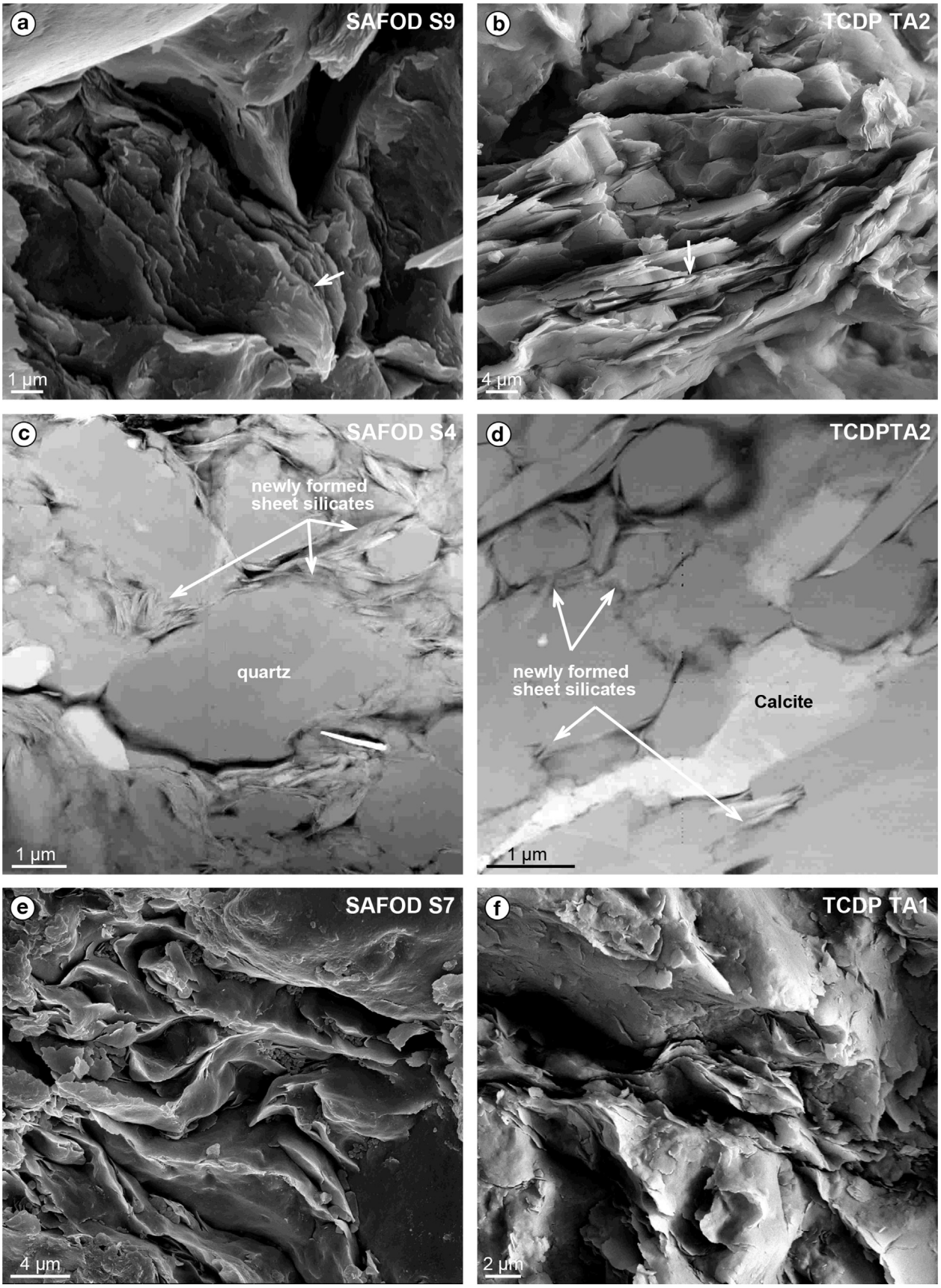

Fig. 11. SEM and TEM photomicrographs of preferred well oriented and randomly clay particles. (a) and (b) well oriented clay stacks in SAFOD and TCDP samples. The preferred oriented clay particles with face-to-face contacts occur only locally (arrow in image). (c) and (d) TEM photomicrographs in SAFOD and TCDP samples showing quartz and feldspar grains surrounded by newly formed clay particles in random orientation. (e) and (f) SEM photomicrographs of folded sheet silicates in SAFOD and TCDP samples.

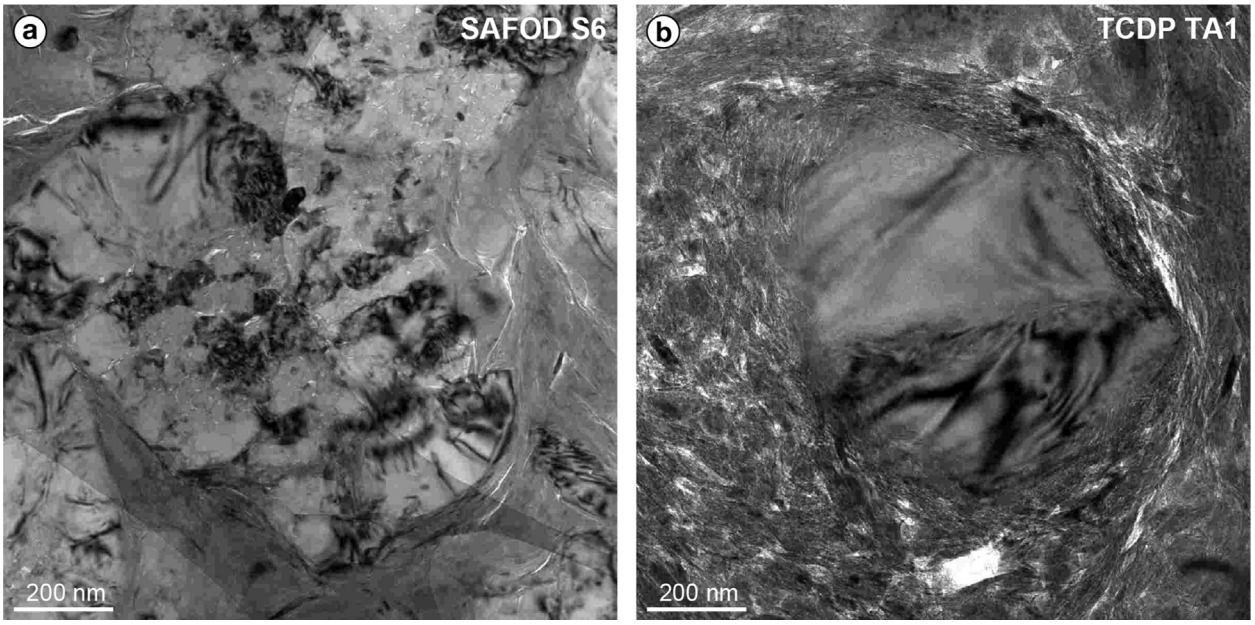

Fig. 12. TEM photomicrographs illustrating clay-clast aggregates with round quartz grains and a cortex made of clay in (a) SAFOD and (b) TCDP samples.

low strain rates during a period of inter-seismic creep (Power and Tullis, 1989) or during slow post-seismic creep respectively (Smith et al., 2011).

5.2.5. Clay-gouge fabric

The presence of a random to weakly oriented clay fabric of highly strained fault gouges is not unique to SAFOD and TCDP fault rocks. Recent analyses conducted on several fault zones (e.g. Alpine Fault, Warr and Cox, 2001; Moab Fault, Solum et al., 2005; Carbonera Fault, Solum and van der Pluijm, 2009; San Andreas Fault, Wenk et al., 2010; Bogd fault, Buatier et al., 2012) also showed only very weak preferred orientation of sheet silicates, regardless of their origin. The lack of a strong fabric in clay-rich fault gouges may be related to localized and narrow shear bands and assisted by the fine grain size of the fault zone materials (Haines et al., 2013). For SAFOD and TCDP samples however, newly formed sheet silicates could also come into play since they are oriented in all possible directions (Fig. 11c and d; compare also Schleicher et al., 2009). In addition, fault-related deformation such as kinking and rotation of sheet silicates on the particle scale may also affect fault gouge fabrics (Fig. 11e and f). Reorientation of clay particles related to deformation and compaction may be associated with a decrease in porosity, and pore pressure increase.

Locally aligned clay particles (mainly smectite–illite) in SAFOD samples are preferentially developed along fracture surfaces (Holdsworth et al., 2011). The coexistence of weak clay fabrics, estimated by X-ray texture measurements, and preferred alignment of clay particles and grains observed under the microscope, is probably related to different scales of observations. For example at mesoscale, Sills et al. (2009) described a strong shape preferred orientation (SPO) of matrix-supported clasts in both creeping zones of the SAF. They concluded from this observation that aseismic creep in the SDZ and CDZ is achieved by distributed shearing.

5.2.6. Clay-clasts aggregates (CCAs)

CCAs have been observed in many clay-bearing fault gouges of seismogenic faults. Warr and Cox (2001) identified a CCA fabric in clay-gouge samples of the Alpine fault in New Zealand where quartz clasts are surrounded by a thick "snowballed" rim of smectite. More recently, CCAs have been recognized in the principal slip zones of the Chelungpu fault in Taiwan (Boullier et al., 2009) and the Tre Monti fault in Apennines, Italy (Smith et al., 2011). Based on high-velocity shear experiments, Boutareaud et al. (2008, 2010) and Ferri et al. (2010, 2011) suggest that CCAs could be a new textural indicator of large slip at co-seismic velocity with thermal pressurization. Boullier et al. (2009) suppose that the presence of CCAs in TCDP samples indicate that the gouge was fluidized as a result of frictional heating and thermal pressurization. Smith et al. (2011) assume a syntectonic origin of the CCAs by localized fluidization at seismic slip velocities within the principal slip zone. On the other hand, rotary shear experiments from Han and Hirose (2012) produced CCAs at slip rates, which are considerably slower than seismic slip rates.

The presence of CCAs in SAFOD samples within and outside of the SAF deforming zones rule out that CCAs were exclusively formed during seismic slip. Our samples also show no evidence for fluidization and thermal pressurization. We suggest that the observed CCAs in fault rock samples are rather formed by rotation of clast (rolling process) over a wide range of slip rates as suggested by Han and Hirose (2012).

6. Conclusions

New microstructural observations from SAFOD and TCDP core samples illustrate that in spite of differences in sample depth/temperature and faulting regime samples from both faults reveal amazing similarities. The use of TEM and SEM combined with focused ion beam sample preparation has been especially powerful for identification of microstructures down to the nm scale. The observations suggest processes such as pressure-solution creep, crystal plastic deformation, and diagenetic crystallization of clay minerals. This concurs with extensive previous work. However, the data do not allow to distinguish unambiguously between seismic slip and aseismic creep. Only frictional melt and co-seismic fluid–rock interactions at high temperatures in TCDP samples of the black gouge zone/PSZ constitute reliable indicators of seismic slip. Mechanical twins in quartz and calcite may also indicate high local stress, possibly as a result of seismic events.

Our microstructural examination has focused on a few selected samples only. For example, Dauphiné twins in quartz grains were only observed in few grains. In the future the methods applied here should be applied to a wider variety of samples from different fault environments to improve our understanding of faulting processes.

Acknowledgments

Diane E. Moore and an anonymous reviewer provided very constructive comments and suggestions that helped to improve this paper. We also would like to thank Andreas Hendrich for help with drafting the figures, Stefan Gehrmann for sample preparation, and Anja Schreiber for TEM foil preparation using FIB technique. A special thanks is due to John Firth, Phil Rumford, Bradley Wymer and Molly Chamberlin for providing samples. This work was supported by Deutsche Forschungsgemeinschaft grant JA 573/4-1. HRW acknowledges support from National Science Foundation (EAR-0836402) and U.S. Department of Energy (DE-FG02-05ER15637) and access to beamline 11-ID-C at the Advanced Photon Source (APS) of Argonne National Laboratory, Office of Science.

Appendix A. Supplementary data

Supplementary data related to this article can be found at http://dx.doi.org/10.1016/j.jsg.2014.04.004.

References

Bachmann, F., Hielscher, R., Schaeben, H., 2010. Texture analysis with MTEX – free and open source software toolbox. Solid State Phenom. 160, 63–68.
Boullier, A.M., 2011. Fault-zone geology: lessons from drilling through the Nojima and Chelungpu faults. Geol. Soc. Lond. Spec. Publ. 359, 17–37.
Boullier, A.M., Yeh, E.C., Boutareaud, S., Song, S.R., Tsai, C.H., 2009. Microscale anatomy of the 1999 Chi-chi earthquake fault zone. Geochem. Geophys. Geosyst. 10 http://dx.doi.org/10.1029/2008GC002252.
Boutareaud, S., Calugaru, D.-G., Han, R., Fabri, O., Mizoguchi, K., Tsutsumi, A., Shimamoto, T., 2008. Clay-clast aggregates: a new textural evidence for seismic fault sliding. Geophys. Res. Lett. 35 http://dx.doi.org/10.1029/2007GL032554.
Boutareaud, S., Boullier, A.-M., Andreani, M., Calugaru, D.-G., Beck, P., Song, S.-R., Shimamoto, D.-G., 2010. Clay clast aggregates: new textural evidence for seismic faulting. J. Geophys. Res. 115 http://dx.doi.org/10.1029/2008JB006254.
Bradbury, K.K., Barton, D.C., Solum, J.G., Draper, S.D., Evans, J.P., 2007. Mineralogical and textural analyses of drill cuttings from the San Andreas Fault Observatory at Depth (SAFOD) boreholes: initial interpretations of fault zone composition and constraints on geological models. Geosphere 3, 299–318.
Bradbury, K.K., Evans, J.P., Chester, J.S., Chester, F.M., Kirschner, D.L., 2011. Lithology and internal structure of the San Andreas Fault at depth based on characterization of Phase 3 whole-rock core in the San Andreas Fault Observatory at Depth (SAFOD) borehole. Earth Planet. Sci. Lett. 304 http://dx.doi.org/10.1016/j.epsl.2011.07.020.
Buatier, M.D., Chauvet, A., Kanitpanyacharoen, W., Wenk, R., Ritz, J.F., Jolivet, M., 2012. Origin and behavior of clay minerals in the Bogd fault gouge, Mongolia. J. Struct. Geol. 34, 77–90.
Chen, J., Yang, X., Ma, S., Spiers, C.J., 2013. Mass removal and clay mineral dehydration/rehydration in carbonate-rich surface exposures of the 2008 Wenchuan Earthquake Fault: geochemical evidence and implication for fault zone evolution and coseismic slip. J. Geophys. Res. 118 http://dx.doi.org/10.1002/jgrb.50089.
Collettini, C., Niemeijer, A., Viti, C., Marone, C., 2009. Fault zone fabric and fault weakness. Nature 462. http://dx.doi.org/10.1038/nature08585.
Di Toro, G., Goldsby, D.L., Tullis, T.E., 2004. Friction falls towards zero in quartz rock as slip velocity approaches seismic rates. Nature 427, 436–439.
Di Toro, G., Hirose, T., Nielsen, S., Pennacchioni, G., Shimamoto, T., 2006. Natural and experimental evidence of melt lubrication of faults during earthquakes. Science 311, 647–649.
Ferri, F., Di Toro, G., Hirose, T., Shimamoto, T., 2010. Evidence of thermal pressurization in high-velocity friction experiments on smectite-rich gouges. Terra Nova 22, 347–353.
Ferri, F., Di Toro, G., Hirose, T., Noda, H., Shimamoto, T., Quaresimin, M., de Rossi, N., 2011. Low-to high-velocity frictional properties of the clay-rich gouges from slipping zone of the 1963 Vaiont slide, northern Italy. J. Geophys. Res. 116 http://dx.doi.org/10.1029/2011JB008338.
Goldsby, D.L., Tullis, T.E., 2002. Low frictional strength of quartz rocks at subseismic slip rates. Geophys. Res. Lett. 29 http://dx.doi.org/10.1029/2002GL015240.
Gratier, J.P., Gamond, J.F., 1990. Transition between seismic and aseismic deformation in the upper crust. Geol. Soc. Lond. Spec. Publ. 54, 461–473.
Gratier, J.-P., Richard, J., Renard, F., Mittempergher, S., Doan, M.-L., Di Toro, G., Hadizadeh, J., Boullier, A.-M., 2011. Aseismic sliding of active faults by pressure solution creep: evidence from the San Andreas Fault Observatory at Depth. Geology 12, 1131–1134.
Hadizadeh, J., Mittempergher, S., Gratier, J.P., Renard, F., Di Toro, G., Richard, J., Babie, H.A., 2012. A microstructural study of fault rocks from the SAFOD: implications for deformation mechanisms and strength of creeping segment of the San Andreas Fault. J. Struct. Geol. 42, 246–260.
Haines, S.H., Kaproth, B., Marone, C., Saffer, D., van der Pluijm, B., 2013. Shear zones in clay-rich fault gouge: a laboratory study of fabric development and evolution. J. Struct. Geol. 51, 206–225.
Han, R., Hirose, T., 2012. Clay-clast aggregates in fault gouge: an unequivocal indicator of seismic faulting at shallow depth? J. Struct. Geol. 43, 92–99.
Hickman, S., Zoback, M., Ellsworth, W., 2004. Introduction to special section: preparing for San Andreas Fault Observatory at Depth. Geophys. Res. Lett. 31 http://dx.doi.org/10.1029/2004GL020688.
Hickman, S., Zoback, M., Ellsworth, W., Bonesse, N., Malin, P., Roecker, S., Thurber, C., 2007. Structure and properties of the San Andreas Fault in Central California: recent results from the SAFOD experiment. Sci. Drill. (Spec. Issue No. 1), 29–32.
Hielscher, R., Schaeben, H., 2008. A novel pole figure inversion method: specification of the MTX algorithm. J. Appl. Crystallogr. 41, 1024–1037.
Hill, M.L., Dibblee, T.W., 1953. San Andreas, Garlock and Big Pine faults. Geol. Soc. Am. Bull. 64, 443–458.
Hirono, T., et al., 2006. Evidence of frictional melting from disk-shaped black material, discovered within the Taiwan Chelungpu Fault System. Geophys. Res. Lett. 33 http://dx.doi.org/10.1029/2006GL027329.
Hirono, T., et al., 2007. Non-destructive continuous physical property measurements of core samples recovered from Hole B, Taiwan Chelungpu-fault Drilling Project. J. Geophys. Res. 122 http://dx.doi.org/10.1029/2006JB004738.
Holdsworth, R.E., van Diggeln, E., Spiers, C., de Bresser, H.J., Walker, R.J., Bowen, L., 2011. Fault rocks from SAFOD core samples. J. Struct. Geol. 33, 132–144.
Hung, J.H., Wu, Y.H., Yeh, E.C., Wu, J.C., the TCDP Scientific Party, 2007. Subsurface structure, physical properties and fault zone characteristics in the scientific drill holes of the Taiwan Chelungpu-fault Drilling Project. Terr. Atmos. Ocean. Sci. 18, 271–293.
Hyndman, R.D., Yamano, M., Oleskevich, D.A., 1997. The seismogenic zone of subduction thrust faults. Island Arc 6, 244–260.
Ikari, M.J., Marone, C., Saffer, D.M., 2011. On the relation between fault strength and frictional stability. Geology 39, 83–86.
Imber, J., Holdsworth, R.E., Smith, S.A.F., Jefferies, S.P., Collettini, C., 2008. Frictional-viscous flow, seismicity and geology of weak faults: a review and future directions. Geol. Soc. Lond. Spec. Publ. 299, 151–173.
Ishikawa, T., et al., 2008. Coseismic fluid-rock interactions at high temperatures in the Chelungpu Fault. Nat. Geosci. 1 http://dx.doi.org/10.1038/ngeo308.
Janssen, C., Wirth, R., Rybacki, E., Naumann, R., Kemmnitz, H., Wenk, H.-R., Dresen, G., 2010. Amorphous material in SAFOD core samples (San Andreas Fault): evidence for crush-origin pseudotachylites? Geophys. Res. Lett. 37 http://dx.doi.org/10.1029/2009GL040993.
Janssen, C., Wirth, R., Reinicke, A., Rybacki, E., Naumann, R., Kemmnitz, H., Wenk, H.-R., Dresen, G., 2011. Nanoscale porosity in SAFOD core samples (San Andreas Fault). Earth Planet. Sci. Lett. 301, 179–189.
Janssen, C., Kanitpanyacharoen, W., Wenk, H.-R., Wirth, R., Morales, L., Rybacki, E., Kienast, M., Dresen, G., 2012. Clay fabrics in SAFOD core samples. J. Struct. Geol. 43, 118–127.
Kirkpatrick, J.D., Rowe, C.D., White, J.C., Brodsky, E.E., 2013. Silica gel formation during fault slip: evidence from rock record. Geology 41, 1015–1018.
Kodaira, S., et al., 2012. Coseismic fault rupture at the trench axis during the 2011 Tohoku-oki earthquake. Nat. Geosci. 5 http://dx.doi.org/10.1038/NGEO1547.
Kuo, L.-W., Song, S.-R., Yeh, E.-C., Chen, H.-F., 2009. Clay mineral anomalies in the fault zone of the Chelungpu Fault, Taiwan, and their implications. Geophys. Res. Lett. 36 http://dx.doi.org/10.1029/2009GL039269.
Kuo, L.-W., Song, S.-R., Huang, L., Yeh, E.-C., Chen, H.-F., 2011. Temperature estimates of coseismic heating in clay-rich fault gouges, the Chelungpu fault zones, Taiwan. Tectonophysics 502, 315–327.
Kuo, L.-W., Hsiao, H.-C., Song, S.-R., Sheu, H.-S., Suppe, J., 2013. Coseismic thickness of principal slip zone from Taiwan Chelungpu fault Drilling Project-A (TCDP-A) and correlated fracture energy. Tectonophysics. http://dx.doi.org/10.1016/j.tecto.2013.07.006.
Lee, J.-C., Chen, Y.-G., Sieh, K., Mueller, K., Chen, W.-S., Chu, H.-T., Chan, Y.-C., Rubin, C., Yeats, R., 2001. A vertical exposure of the 1999 surface rupture of the Chelungpu fault at Wufeng, Western Taiwan: structural and paleoseismic implications for an active thrust fault. Bull. Seismol. Soc. Am. 91, 914–929.
Lin, A., 1994. Glassy pseudotachylites veins from the Fuyun fault zone, northwest China. J. Struct. Geol. 16, 71–83.
Lockner, D.A., Morrow, C., Moore, D., Hickman, S., 2011. Low strength of deep San Andreas Fault gouge from SAFOD core. Nature 472. http://dx.doi.org/10.1038/nature09927.
Ma, K., et al., 2006. Slip zone and energetics of large earthquake from the Taiwan Chelungpu-fault Drilling project. Nature 444, 473–476.
Marone, C., Saffer, D.M., 2007. Fault friction and the upper transition from seismic to aseismic faulting. In: Dixon, T.H., Moore, J.C. (Eds.), The Seismogenic Zone of Subduction Thrust Faults. Columbia University Press, ISBN 978-0-231-13866-6, p. 692.

Mittempergher, S., Di Toro, G., Gratier, J.P., Hadizadeh, J., Smith, S.A.F., Spiess, R., 2011. Evidence of transient increases of fluid pressure in SAFOD phase III cores. Geophys. Res. Lett. 38, L03301 http://dx.doi.org/10.1029/2010GL046129.
Moore, D.E., Lockner, D.A., 2011. Frictional strengths of talc-serpentine and talc-quartz mixtures. J. Geophys. Res. 116 http://dx.doi.org/10.1029/2010JB007881.
Moore, D.E., Rymer, M.J., 2007. Talc-bearing serpentinite and the creeping section of the San Andreas Fault. Nature 448. http://dx.doi.org/10.1038/nature06064.
Moore, D.E., Rymer, M.J., 2012. Correlation of clayey gouge in a surface exposure of serpentinite in the San Andreas Fault with gouge from the San Andreas Fault Observatory at Depth (SAFOD). J. Struct. Geol. 38, 51–60.
Mori, J., Kano, Y., Yanagidani, T., Ito, H., 2008. Temperature measurement in ~1 km borehole of TCDP. ftp://ftp-eost.u-strasbg.fr/…MeasuringTemperature/t….
Otsuki, K., Uduki, T., Monzawa, N., Tanaka, H., 2005. Clayey injection veins and pseudotachylite from two boreholes penetrating the Chelungpu Fault, Taiwan: their implication for the contrastive seismic slip behaviors during the 1999 Chi-Chi earthquake. Island Arc 14, 22–26.
Otsuki, K., Hirono, T., Omori, M., Sakaguchi, M., Tanigawa, W., Lin, W., Soh, W., Rong, S.-S., 2009. Analyses of pseudotachylites from Hole-B of Taiwan Chelungpu Fault Drilling Project (TCDP); their implications for seismic slip behaviors during the 1999 Chi-Chi earthquake. Tectonophysics 469, 13–24.
Ozawa, S., et al., 2011. Coseismic and postseismic slip of the 2011 magnitude-9 Tohoku-Oki earthquake. Nature 475, 373–376.
Power, W.L., Tullis, T.E., 1989. The relationship between slickenside surfaces in fine grained quartz and the seismic cycle. J. Struct. Geol. 11, 879–893 http://dx.doi.org/10.1016/0191-8141(89)90105-3.
Richard, J., Gratier, J.-P., Doan, M.-L., Boullier, A.M., Renard, F., 2013. Time and space evolution of an active creeping fault zone: insights from the brittle and ductile microstructures in the San Andreas Fault Observatory at Depth. isterre.fr/docrestreint.api/ … /richard13_jgr _safod.pdf.
Rietveld, H.M., 1969. A profile refinement method for nuclear and magnetic structures. J. Appl. Crystallogr. 2, 65–71.
Rybacki, E., Janssen, C., Wirth, R., Chen, K., Wenk, H.-R., Stromeyer, D., Dresen, G., 2011. Low-temperature deformation in calcite veins of SAFOD core samples (San Andreas Fault) — microstructural analysis and implications for fault rheology. Tectonophysics 509, 107–119.
SAFOD Core Photo Atlas, 2010. Photographic Atlas of the SAFOD Phase 3 Cores, version 4. www.earthscope.org.
Saffer, D.M., Marone, C., 2003. Comparison of smectite and illite frictional properties: application to the updip limit of the seismogenic zone along subduction megathrusts. Earth Planet. Sci. Lett. 215, 219–235.
Schleicher, A.M., Warr, L.N., van der Pluijm, B.A., 2009. On the origin of mixed-layered clay minerals from the San Andreas Fault at 2.5–3 km vertical depth (SAFOD drillhole at Parkfield, California). Contrib. Mineral. Petrol. 157, 173–187.
Schleicher, A.M., van der Pluijm, B.A., Warr, L.N., 2010. Nanocoatings of clay and creep of the San Andreas Fault at Parkfield. Geology 38, 667–670.
Schleicher, A.M., van der Pluijm, B.A., Warr, L.N., 2012. Chlorite-smectite clay minerals and fault behavior: new evidence from the San Andreas Fault Observatory at Depth (SAFOD) core. Lithosphere 4, 209–220.
Sibson, R.H., 1975. Generation of pseudotachylite by ancient seismic faulting. Geophys. J. R. Astr. Soc. 43, 775–794.
Sills, D.W., Chester, J.S., Chester, F.M., 2009. Shape preferred orientation of porphyroclasts in the active gouge zone of the San Andreas Fault at SAFOD. Eos Trans. AGU 90 (52). Fall Meet. Suppl., Abstract T43A-2057.
Smith, S., Billi, A., Di Toro, G., Spiess, R., 2011. Principal slip zones in Limestones: microstructural characterization and implications for the seismic cycle (Tre Monti Fault, central Apennines, Italy). Pure Appl. Geophys. 168, 2365–2393.
Solum, J.G., van der Pluijm, B.A., 2009. Quantification of fabrics in clay gouge from the Carboneras fault, Spain and implications for fault behavior. Tectonophysics 475, 554–562.
Solum, J.G., van der Pluijm, B.A., Peacor, D.R., 2005. Neocrystallization, fabrics and age of clay minerals from the exposure the Moab Fault, Utah. J. Struct. Geol. 27, 1563–1576.
Sone, H., Yeh, E.C., Nakaya, T., Hung, J.H., Ma, K.F., Wang, C.Y., Song, S.R., Shimamoto, T., 2007. Mesoscopic structural observations of cores from the Chelungpu fault system, Taiwan Chelungpu-fault Drilling Project Hole-A, Taiwan. Terr. Atmos. Ocean. Sci. 18, 359–377 http://dx.doi.org/10.3319/TAO.2007.18.23598TCDP9.
Song, S.R., Kuo, L.W., Yeh, E.C., Wang, C.Y., Hung, J.H., Ma, K.F., 2007. Characteristic of the lithology, fault-related rocks and fault zone structure in TCDP Hole-A. Terr. Atmos. Ocean. Sci. 18, 243–269.
Titus, S.J., De Mets, C., Tikoff, B., 2006. Thirty-five-year creep rates for the creeping segment of the San Andreas fault and the effects of the 2004 Parkfield earthquake: constraints from alignment arrays, continuous Global Positioning System, and creepmeters. Bull. Seismol. Soc. Am. 96, 250–S268 http://dx.doi.org/10.1785/0120050811.
Toy, V., Ritchi, S., Sibson, R., 2011. Diverse habitats of pseudotachylites in the Alpine Fault Zone and relationships to current seismicity. Geol. Soc. Lond. Spec. Publ. 359 (1), 115–133.
Ujiie, K., Yamaguchi, H., Sakaguchi, A., Toh, S., 2007. Pseudotachylitess in an ancient accretionary complex and implications for melt lubrication during subduction zone earthquakes. J. Struct. Geol. 29, 599–613.
Van der Pluijm, B., 2012. Natural fault lubricants. Nat. Geosci. 4, 217–218.
Vasin, R., Wenk, H.-R., Kanitpanyacharoen, W., Matthies, S., Wirth, R., 2013. Anisotropy of Kimmeridge shale. J. Geophys. Res. 118, 1–26 http://dx.doi.org/10.1002/jgrb.50259.
Warr, L.N., Cox, S., 2001. Clay mineral transformation and weakening mechanisms along the Alpine Fault, New Zealand. In: Holdsworth, R.E., Strachan, R.A., Magloughlin, J.F., Knipe, R.J. (Eds.), The Nature and Tectonic Significance of Fault Weakening, Geological Society, London, Special Publication, vol. 186, pp. 85–1001.
Wenk, H.R., 1978. Are pseudotachylites products of fracture of fusion? Geology 6, 507–511.
Wenk, H.R., Johnson, L.R., Ratschbacher, L., 2000. Pseudotachylites in the eastern Peninsular ranges of California. Tectonophysics 321, 253–277.
Wenk, H.-R., Voltolini, M., Mazurek, M., Van Loon, L.R., Vinsot, A., 2008. Preferred orientations and anisotropy in shales: Callovo-Oxfordian shale (France) and Opalinus Clay (Switzerland). Clays Clay Miner. 56, 285–306.
Wenk, H.-R., Kanitpanyacharoen, W., Voltolini, M., 2010. Preferred orientation of phyllosilicates: comparison of fault gouge, shale and schist. J. Struct. Geol. 32, 478–489.
Wenk, R., Janssen, C., Kenkmann, T., Dresen, G., 2011. Mechanical twinning in quartz: shock experiments, impact, pseudotachylites and fault breccias. Tectonophysics 510, 69–79.
Wirth, R., 2004. A novel technology for advanced application of micro- and nano-analysis in geosciences and applied mineralogy. Eur. J. Mineral. 16, 863–876.
Wirth, R., 2009. Focused Ion Beam (FIB) combined with SEM and TEM: advanced analytical tools for studies of chemical composition, microstructure and crystal structure in geomaterials on a nanometre scale. Chem. Geol. 261, 217–229.
Ye, E.C., et al., 2007. Core description and characteristics of fault zones from Hole-A of the Taiwan Chelungpu-fault drilling project. Terr. Atmos. Ocean. Sci. 18, 327–357 http://dx.doi.org/10.3319/TAO.2007.18.2.327(TCDP).
Yu, S.B., et al., 2001. Preseismic deformation and co-seismic displacement associated with the 1999 Chi-Chi Taiwan earthquake. Bull. Seismol. Soc. Am. 91, 995–1012 http://dx.doi.org/10.1785/0120000722.
Zoback, M.D., Hickman, S.H., Ellsworth, W., 2007. Proposal for the National Science Foundation, Earth Scope, Facility Operation and Maintenance.
Zoback, M.D., Hickman, S.H., Ellsworth, W., 2010. Scientific drilling into the San Andreas Fault Zone. Eos Trans. AGU 91, 197–204.
Zoback, M.D., Hickman, S.H., Ellsworth, W., the SAFOD Science Team, 2011. Scientific drilling into the San Andreas Fault Zone – an overview of SAFOD's first five years. Sci. Drill. 11, 14–28.